Graphical Abstract

Click here to download Graphical Abstract Graphical abstract 300dpi.tif

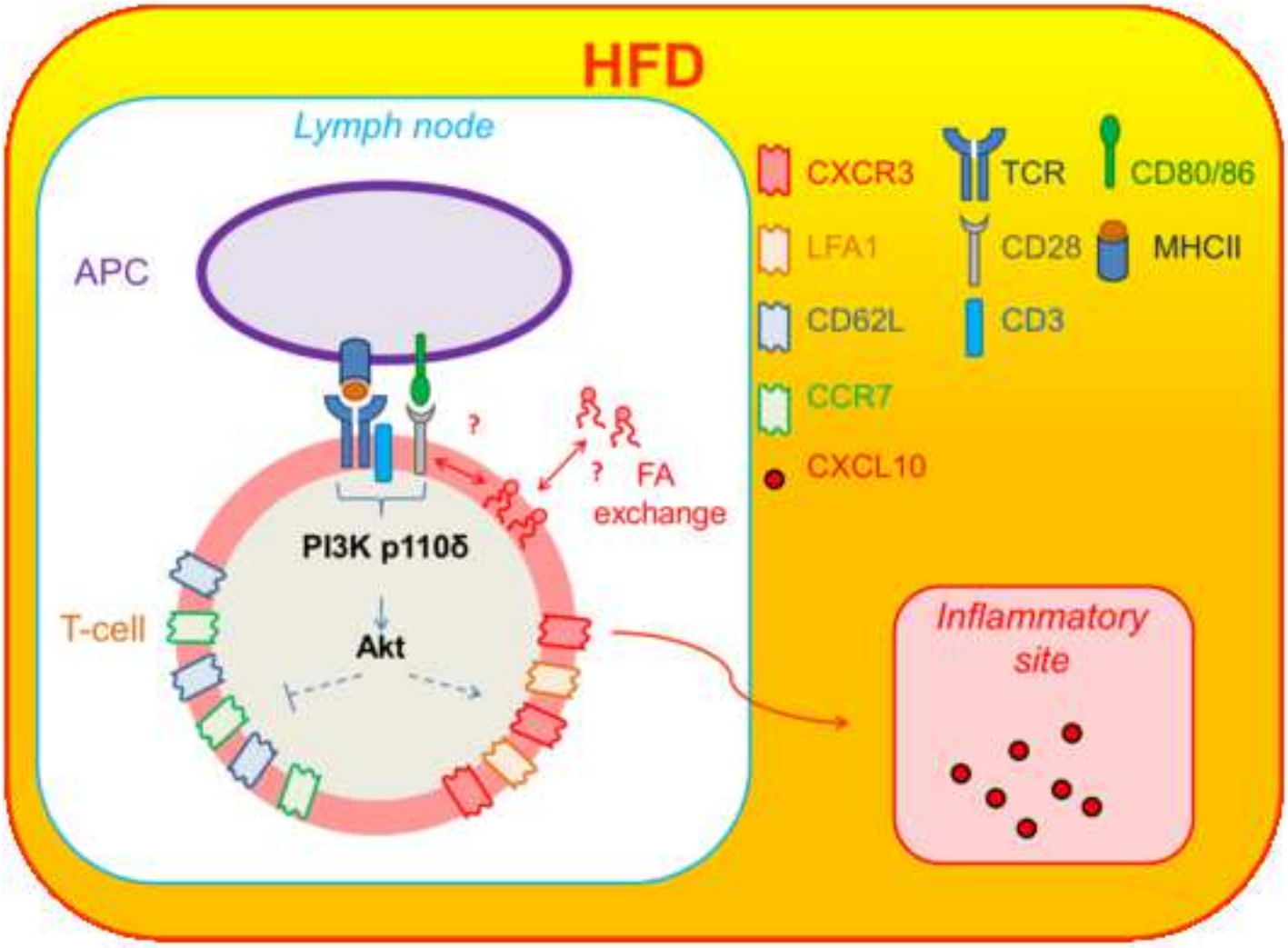

Obesity-induced metabolic stress leads to biased effector memory CD4$^+$ T cell differentiation via PI3K p110δ/Akt-mediated signals

Claudio Mauro[1*#+], Joanne Smith[1*], Danilo Cucchi[1,2], David Coe[1], Hongmei Fu[1], Fabrizia Bonacina[3], Andrea Baragetti[3], Gaia Cermenati[3], Donatella Caruso[3], Nico Mitro[3], Alberico L. Catapano[3,4], Enrico Ammirati[5], Maria P. Longhi[1], Klaus Okkenhaug[6], Giuseppe D. Norata[3,7] and Federica M. Marelli-Berg[1#]

[1] William Harvey Research Institute, Barts and The London School of Medicine and Dentistry, Queen Mary University of London, London, UK

[2] Istituto Pasteur, Fondazione Cenci Bolognetti, Rome, Italy

[3] Department of Pharmacological and Biomolecular Sciences, Università degli Studi di Milano, Milan, Italy

[4] IRCCS Multimedica, Milan, Italy

[5] De Gasperis Cardio Center, Niguarda Ca' Granda Hospital, Milan, Italy

[6] Laboratory of Lymphocyte Signalling and Development, Babraham Institute, Cambridge, UK

[7] School of Biomedical Sciences, Curtin Health Innovation Research Institute, Curtin University, Perth, Western Australia

* Equal contribution

[#] Correspondence: c.mauro@qmul.ac.uk or f.marelli-berg@qmul.ac.uk

[+] Lead contact

SUMMARY

Low-grade systemic inflammation associated to obesity leads to cardiovascular complications, caused partly by infiltration of adipose and vascular tissue by effector T cells. The signals leading to T cell differentiation and tissue infiltration during obesity are poorly understood.

We tested whether saturated fatty acid-induced metabolic stress affects differentiation and trafficking patterns of $CD4^+$ T cells. Memory $CD4^+$ T cells primed in high-fat diet-fed donors preferentially migrated to non-lymphoid, inflammatory sites, independent of the metabolic status of the hosts. This was due to biased $CD4^+$ T cell differentiation into $CD44^{hi}$-$CCR7^{lo}$-$CD62L^{lo}$-$CXCR3^+$-$LFA1^+$ effector memory-like T cells upon priming in high-fat diet-fed animals. Similar phenotype was observed in obese subjects in a cohort of free-living people.

This developmental bias was independent of any crosstalk between $CD4^+$ T cells and dendritic cells and was mediated via direct exposure of $CD4^+$ T cells to palmitate, leading to increased activation of a PI3K p110δ/Akt-dependent pathway upon priming.

INTRODUCTION

Obesity is a major and ever growing burden on public health worldwide. Individuals with obesity are at increased risk of several health conditions including type 2 diabetes, dyslipidaemia, liver steatosis, hypertension, cardiovascular disease, osteoarthritis, as well as various forms of cancer (Faulds and Dahlman-Wright, 2012; Mauro and Marelli-Berg, 2012; Norata et al., 2015). A strong link between obesity and the establishment of chronic systemic inflammation has recently emerged (Bjorndal et al., 2011), and is often related to increased expression of adipokines (i.e. leptin, chemerin, resistin), myokines and pro-inflammatory mediators [i.e. tumour necrosis factor (TNF)-α, interleukin (IL)-1 and IL-6], and decreased expression of the anti-inflammatory cytokine, adiponectin (Norata et al., 2015). In obesity, activated immune cells [including T cells, macrophages and dendritic cells (DC)] infiltrate adipose tissue, promoting in turn the production of pro-inflammatory cytokines such as TNF-α, IL-6, resistin and monocyte chemotactic protein-1 (MCP-1/CCL2), (Mathis and Shoelson, 2011; Norata et al., 2015). This process is thought to underlay the activation of both the innate and adaptive arms of the immune system, which results in the chronic inflammatory response observed in obese subjects (Larbi et al., 2008; Shaw et al., 2010). While T cells, B cells, macrophages, neutrophils and mast cells are increased in number in the visceral adipose tissue (AT) of obese individuals, specific subsets of T cells [helper T cell type (Th2), regulatory T cells and invariant natural killer T (iNKT)] cells as well as eosinophils are reduced (Cildir et al., 2013). Obesity-related inflammation, caused by excessive and inappropriate activation of the immune system, is pivotal to disease progression and the development of complications such as atherosclerosis and type II diabetes (Norata et al., 2015). T lymphocytes play a major role in the development of these inflammatory processes both via direct cytotoxic activities and secretion of cytokines that influence the severity and outcome of the inflammatory reaction (Hamann et al., 2000). Based on the observation that T cells in the adipose tissue display specific T cell receptor (TCR) rearrangements it has

been proposed that obesity might be associated with an autoimmune response (Gerriets and Rathmell, 2012).

The mechanisms of enhanced T cell activation and tissue infiltration during obesity, however, remain elusive.

Altered antigen presentation by DC has been proposed to underlie the activation of adaptive immunity observed in dyslipidaemia. Although AT-derived DC in obesity display an immature phenotype with lower expression of activation markers such as CD40, CD80 and CD86 (Chen et al., 2014), they promote the differentiation of pro-inflammatory interferon (IFN)γ^+ $CD4^+$ T cells (Chen et al., 2014).

A very recent report has implicated dietary long- and medium-chain fatty acids (FA) in T cell differentiation towards Th1 and Th17 subsets in autoimmune responses of the central nervous system (Haghikia et al., 2015), however whether FA can directly affect T cell activation and differentiation towards specific cell subsets during metabolic overload remains to be established.

In this study, we investigated the phenotypic, functional and migratory features of memory $CD4^+$ T cells in experimental models of saturated FA-induced metabolic stress, as well as in human $CD4^+$ T cells obtained from individuals in a large cohort of free-living people [Progressione della Lesione Intimale Carotidea (PLIC) study: n=2,606]. Mechanistic studies show that direct exposure of $CD4^+$ T cells to saturated FA, i.e. palmitate, which is enriched in high-fat diet (HFD), induces $CD4^+$ T cells to acquire a specific $CD44^{hi}$-$CCR7^{lo}$-$CD62L^{lo}$-$CXCR3^+$-$LFA1^+$ pro-inflammatory functional phenotype via enhanced engagement of a PI3K p110δ/Akt-dependent pathway upon priming, but independent of the modality of antigen presentation by DC.

RESULTS

Priming following HFD induces differentiation of a CD4$^+$ T cell population that readily migrates to inflamed, non-lymphoid tissues independent of the metabolic status of the host.

Given that lymphocyte infiltration of non-lymphoid tissues is a prominent feature of chronic inflammation, we first assessed whether HFD-induced metabolic stress directly promotes the generation of T cell populations with specific migratory features. To this aim, memory CD4$^+$ T cells were generated in Rag2-deficient TCR transgenic Marilyn female mice, which harbour monoclonal CD4$^+$ T cells specific for the male antigen H-Y (Lantz et al., 2000), by *i.p.* injection of male splenocytes (Robertson et al., 2007). CD4$^+$ T cells were then isolated from the lymph nodes of donors fed 8-week chow (CD) or high-fat (HFD) diet, and adoptively transferred in HFD- or CD-fed (*i.e.* fed chow or high-fat diet for 8 weeks, respectively) C57BL/6 male recipients that had been *i.p.* injected with zymosan and IFNγ 48 hours earlier to induce localized inflammation (Fig S1A-C), (Fu et al., 2014). *In vivo*-primed CD4$^+$ T cells isolated from HFD donors exited from the blood circulation of CD recipients with a kinetic 24 hours faster than their CD counterpart (Fig 1A). CD4$^+$ T cells that were primed in HFD donors also trafficked preferentially to the non-lymphoid, inflamed sites (peritoneal cavity) of both HFD and CD recipients (Fig 1B). In contrast, primed CD4$^+$ T cells from CD donors preferentially localized to the mesenteric lymph nodes of both CD and HFD recipients (Fig 1C). No difference in CD4$^+$ T cell localization to the spleen was observed when comparing equal numbers of adoptively transferred CD and HFD donors (Fig 1D). These results indicate that memory T cell populations induced in CD or HFD-fed animals are characterized by different trafficking patterns.

To establish the pathophysiological relevance of these differential trafficking patterns, we performed HY-mismatched skin grafts whereby male skin was implanted on the upper right back of CD or HFD-fed Marilyn female recipients. We found that rejection of HY-

mismatched skin was significantly accelerated in HFD as compared to CD female recipients (Fig 1E), (Molinero et al., 2016). Activation of $CD4^+$ T cells and their localization to the graft are known to be instrumental to rejection in this system (Chen et al., 2003). Indeed, we observed that HY-mismatched skin graft rejection was completely abrogated in Rag2KO mice (that are deficient for mature T and B cells) independent of the diet they received (Fig S1D). Reconstitution of HFD Rag2KO mice with $CD4^+$ T cells isolated from Marilyn mice resulted in a rapid rejection of the transplanted male-derived skin (Fig S1D), showing the crucial role these cells play in such system. These findings support the conclusion that biased differentiation of $CD4^+$ T cells towards a pro-inflammatory effector memory phenotype takes place during HFD-induced metabolic stress.

HFD-induced metabolic stress promotes the differentiation of primed $CD4^+$ T cells to a $CXCR3^+$-$LFA1^+$ effector memory-like phenotype in mice.

Based on the distinct homing preferences of memory T cells generated in HFD- or CD-fed animals and the stronger immune response elicited in HFD animals, we asked whether a biased differentiation of activated $CD4^+$ T cells towards a pro-inflammatory phenotype – and associated homing receptors - takes place upon priming following HFD-induced metabolic stress.

Using the same immunization procedure as that used for the experiments presented in Fig 1A-D, we found that HFD-fed hosts displayed an increase in the size of the $CD44^{hi}$-$CCR7^{lo}$-$CD62L^{lo}$-$CXCR3^+$-$LFA1^+$ effector memory-like $CD4^+$ T cell population and no difference in the $CD44^{hi}$-$CCR7^{hi}$-$CD62L^{hi}$ central memory $CD4^+$ T cells as compared to $CD4^+$ T cells primed in CD-fed mice (Fig 2A-D and S2A-D). In contrast, the size of naïve T cells was reduced in HFD (Fig 2A-B and S2A-B). These data suggest a preferential $CD4^+$ T cell differentiation towards an effector memory phenotype under HFD regimen in concomitance with a reciprocal reduction of the naïve cell population without affecting the size of the central memory pool. No difference was observed in the expression of the activation markers

CD25 and CD44 (Fig 2E-F and S2E-F) by memory $CD4^+$ T cells activated in CD or HFD hosts, indicative of similar priming efficiency in either metabolic background. In agreement with the observed phenotypes, a significantly larger fraction of *in vivo*-primed $CD4^+$ T cells isolated from the lymph nodes of HFD mice migrated in response to the pro-inflammatory chemokine CXCL10 (a CXCR3 ligand) in *ex vivo* chemotaxis assays, whilst most *in vivo*-primed $CD4^+$ T cells isolated from the lymph nodes of CD mice migrated to the homeostatic lymphoid tissue chemokines CCL19 and CCL21 (ligands of CCR7), (Fig 2G). To investigate the cellular sources of CXCL10 *in vivo*, mice received an *i.p.* injection of IFNγ. 48 hours later intracellular staining of CXCL10 in a number of immune cell populations retrieved from the peritoneal cavity was performed. We chose this system because of its relevance to the peritoneal recruitment system shown in Fig 1A-D. Data indicate that resident (peritoneal) and to a less extent infiltrating (monocyte-derived) macrophages are main sources of CXCL10 in this model (Fig S2G-H). Furthermore, we observed an increase in the $IFN\gamma^+$ and $IL4^+$ populations upon priming following HFD (Fig 2H-I).

Our findings are in line with previous work showing that increased expression of CXCR3 in inflammatory conditions, such as obesity and atherosclerosis, drives accumulation of inflammatory T cells in fat sites. Indeed, CXCR3- or CXCL10-deficient mice are protected from obesity- and atherosclerosis-induced inflammation in association with reduced accumulation of effector T cells and macrophages in AT and atherosclerotic plaques (Gupta et al., 1997; Rocha et al., 2014; Veillard et al., 2005).

Obesity is associated with increased numbers of circulating CXCR3$^+$ effector memory T cells in humans.

A cohort of 1,172 subjects was selected by probability sampling from a large survey of free-living people (PLIC study: n=2,606; average age 66 years). The selected cohort was representative of the entire PLIC cohort in terms of age, gender and clinical parameters

according to the Kolmogorov-Smirnov test; individuals were stratified in three groups (*i.e.* lean, overweight and obese), based on body mass index (BMI), and a number of biochemical and cellular markers of their peripheral blood were analysed (Table S1). In particular, this analysis revealed increased total lymphocyte counts in the blood of overweight and obese as compared to lean individuals (Table S1, Fig 3A). From this cohort, a detailed immunophenotype was performed in a group of n=187 subjects. Again, these individuals were selected by probability sampling and were representative of the entire cohort according to the Kolmogorov-Smirnov test. Specific subsets of circulating $CD4^+$ T cells were assessed by 10-parameter/8-color polychromatic flow-cytometry with CD3, CD4, CD45RO, CD45RA, CCR7, CCR5, CXCR3, and HLA-DR as markers. The main $CD4^+$ T cell subsets present in the blood were identified by flow cytometry based on a well-defined gating strategy (Fig S3A-B). The percentage of total T-helper lymphocytes was equal in the three groups (Fig 3B); however, we found a strong association of the obese condition with reduced naïve T cells and increased effector memory T cells (Fig 3C-D).

To gain further insights in to the relationship in humans between obesity and the effector memory phenotype of $CD4^+$ T cells we focused on the few very obese patients in our cohort (BMI>35kg/m2, n=5) and observed that percentage of effector memory T cells was raised to 18.2% [11.2-21.3] as compared to 13.4% [8.8-18.25] of the entire obese population (Fig 3D-E) and to 10.2% [8.4-12.5] of the lean population (see Fig 3D). To address the potential link of this phenotype with obesity-related chronic inflammation, we also analyzed the blood levels of C reactive protein (CRP) in the lean, overweight and obese subjects. As expected CRP levels rose progressively with increasing BMI (Fig S4A), corroborating the correlation between obesity and inflammation. However, no significant correlation was observed between CRP levels and effector memory T cells (Fig S4B). Furthermore, no correlation between fasting glucose levels and effector memory T cells was observed (p=0.117). Also, effector memory T cells were not significantly increased in type 2 diabetes subjects (n=13) as compared to the rest of the subjects in the cohort (p= 0.069).

The body mass fat distribution of each individual was also analysed by dual-energy X-ray absorptiometry (Fig S4C) and the resulting android/gynoid ratio was correlated with the percent of various T cell subsets. The android/gynoid ratio correlated negatively with the naïve T cell subset (Fig 3F) and positively with the $CXCR3^+$ effector memory T cell subset (Fig 3G-H). No significant correlation between the android/gynoid ratio and $HLADR^+$ or $CCR5^+$ effector memory T cell subsets was observed instead (Fig S4D-E).

Antigen presentation by DC from metabolically stressed donors does not affect T cell differentiation to a pro-inflammatory effector memory-like phenotype.

Prompted by previous suggestions that altered antigen presentation by DC might affect T cell activation during metabolic stress (Chen et al., 2014; Shamshiev et al., 2007), we assessed the effect of splenic DC purified from HFD or CD animals on T cell activation and differentiation. We found that *in vitro* co-cultures of DC isolated from the spleen of CD-fed C57BL/6 male mice with $CD4^+$ T cells obtained from the lymph nodes of CD-fed Marilyn mice induced a strong proliferative response of Marilyn $CD4^+$ T cells, which was reduced when $CD4^+$ T cells were isolated from donors fed HFD (Fig 4A and S5A). In contrast, DC purified from the spleen of C57BL/6 male mice fed HFD were significantly less effective in promoting $CD4^+$ T cell proliferation compared to their 'CD-fed' counterpart, irrespective of the T cell metabolic status [i.e. CD or HFD $CD4^+$ T cell donors (Fig 4A and S5A), in line with previous reports (Shamshiev et al., 2007)]. These data suggest that the metabolic status of DC plays a role in determining their ability to promote $CD4^+$ T cell proliferation. However, it did not affect the differentiation of $CD4^+$ T cells to central versus effector memory phenotype. Indeed, HFD $CD4^+$ T cells showed higher percent of $CD44^{hi}$-$CCR7^{lo}$-$CD62^{lo}$-$CXCR3^+$ cells as compared to CD $CD4^+$ T cells (consistent with Fig 2A-C) independent of whether they were co-cultured with DC from HFD- or CD-fed donors (Fig 4B). Similar results were obtained *in vivo* when $CD4^+$ T cells isolated from female Marilyn mice were co-injected with DC from HFD or CD C57BL/6 male donors in C57BL/6 female recipients (i.e. reduced $CD4^+$ T cell

proliferation in the presence of DC from HFD-fed mice and no effect on central memory versus effector memory differentiation; Fig S5B-C).

In line with previous reports (Shamshiev et al., 2007), DC isolated from HFD-fed mice showed impaired activation as indicated by reduced expression of the activation markers CD80 and CD86 as compared to lean DC (Fig 4C).

CD4$^+$ T cell exposure to saturated FA causes enhanced activation of a PI3K p110δ/Akt-dependent pathway upon priming.

Having ruled out a possible role for altered antigen presentation by DC in biasing CD4$^+$ T cell differentiation to the CXCR3$^+$ effector memory phenotype observed during HFD-induced metabolic stress, we sought to establish whether CD4$^+$ T cell intrinsic alterations were responsible for this event by interrogating pathways controlling nutrient responses in T cells. PI3K/Akt and mammalian target of rapamycin complexes (mTORC1 and mTORC2) are known to be rapidly activated upon T cell priming and control transcriptional and metabolic programs that sustain cell activation (Finlay et al., 2012; Macintyre et al., 2011). We found a substantial increase in the levels of Akt activation (phosphorylation at serine 473, a target of mTORC2) in *in vivo*-primed CD4$^+$ T cells isolated from the lymph nodes of HFD- as compared to CD-fed mice (Fig 5A, compare lanes 6-8 versus 1-2). Similar results were obtained with CD4$^+$ T cells isolated from the peripheral blood of obese versus lean individuals selected from the PLIC cohort (Fig 5B). In contrast, threonine 308 on Akt and the mTORC1 target S6 did not undergo any significant modulation when comparing *in vivo*-primed CD4$^+$ T cells isolated from the lymph nodes of HFD or CD mice (Fig 5A and S6A). In line with recent literature (Finlay et al., 2012; Macintyre et al., 2011) our data suggest that CD4$^+$ T cell priming following HFD regimen triggers a PI3K/Akt pathway via mTORC2 but does not result in downstream mTORC1 activation.

A recent report has implicated direct signaling induced by dietary FA in T cell differentiation in the gut, with middle- and long-chain FA supporting Th1 and Th17 cell

differentiation and short-chain FA promoting Treg cell development (Haghikia et al., 2015). In line with previous evidence, using lipidomic analysis we found that HFD alters the fatty acid and phospholipid profile of T cells (Fig S6B), resulting in increased membrane fluidity (Fig 5C). This might underlay a reduced threshold for TCR clustering and activation in HFD (Swamy et al., 2016). Indeed, ImageStream analysis enabled us to observe that *in vitro* activation of T cells isolated from HFD as compared to CD mice results in increased aggregation of Cholera enterotoxin (CTx) B staining (Fig 5D and S6C), indicative of enhanced formation of lipid rafts, a key signaling event downstream of TCR engagement (Viola et al., 1999). The saturated FA palmitate has been shown to directly promote the activation of the inflammasome via NLRP3 and ASC (Wen et al., 2011) and of the Toll-like receptor (TLR) 4/MyD88 pathway (Eguchi et al., 2012). We therefore reasoned that the observed effector memory phenotype and enhanced activation of the PI3K/Akt pathway during $CD4^+$ T cell 'HFD priming' could be due to a direct effect of the saturated FA palmitate, whose levels increase during HFD. Mirroring the results shown in Fig 2A-D, we found that palmitate enriched diet (PED)-fed animals displayed an increase in the size of the $CD44^{hi}$- $CCR7^{lo}$-$CD62L^{lo}$-$CXCR3^+$-$LFA1^+$ effector memory-like $CD4^+$ T cell population and no difference in the $CD44^{hi}$-$CCR7^{hi}$-$CD62L^{hi}$ central memory $CD4^+$ T cells as compared to $CD4^+$ T cells primed in the corresponding palmitate control diet (PCD) fed-mice (Fig 5E-H). In contrast, the size of the naïve T cell subset was reduced upon PED (Fig 5E-H). Further, $CD4^+$ T cells were cultured over-night with IL-7 in the presence or absence of either palmitic or linoleic acid at a concentration which mirrors plasma levels in obese individuals (200μM), followed by activation with anti-CD3 and anti-CD28 for the indicated time points. As shown in Fig 5I, $CD4^+$ T cell activation in the presence of palmitic acid for 2 hours showed a trend of enhanced Akt activation compared to linoleic acid or untreated control without any modulation of S6. In similar experimental settings, only $CD4^+$ T cell activation in the presence of palmitic but not stearic acid for 48 hours led to reduced levels of CCR7 and CD62L mRNA (Fig 5J). In line with previous reports (Eguchi et al., 2012; Wen et al., 2011) these data suggest the existence of specific sensing mechanisms for palmitate.

To further link the activation of the PI3K/Akt pathway to the observed specific $CD4^+$ T cell differentiation during 'HFD priming', we activated $CD4^+$ T cells via CD3/CD28 antibody ligation in the presence or absence of the Akt activator SC79. As expected, such treatment led to marked Akt phosphorylation (Fig S6D). Importantly, enhanced Akt activation led to reduced levels of CCR7 and CD62L mRNA as well as CCR7 protein (Fig 5K-L), indicating that increased Akt activation during $CD4^+$ T cell priming directly promotes the pathway leading to the differentiation of effector memory-like T cells.

The PI3K/Akt pathway is key for the differentiation of $CXCR3^+$ effector memory T cells.

We addressed the question as to whether enhanced PI3K/Akt activation as we observed during 'HFD priming' in $CD4^+$ T cells was instrumental to the biased T cell differentiation to the observed $CXCR3^+$ effector memory phenotype. The p110δ subunit of PI3K is crucial for correct TCR signaling and T cell activation (Okkenhaug et al., 2002). Furthermore, p110δ engagement during T cell priming is instrumental for Akt activation and differentiation towards an effector memory phenotype, at least in $CD8^+$ T cells (Finlay et al., 2012; Macintyre et al., 2011). We therefore took genetic and pharmacologic approaches to selectively target p110δ and Akt activities *in vivo*. First, allogeneic $CD4^+$ T cells were primed *in vivo* in HFD-fed $p110\delta^{D910A}$ (expressing kinase-dead p110δ) or wild-type (WT) mice. Genetic inhibition of p110δ activity completely reversed $CD4^+$ effector memory differentiation in HFD-fed animals (Fig 6A-D). This was accompanied by a reduction of both Akt activation on serine 473 (Fig 6E) and migration in response to the chemokine CXCL10 (Fig 6F). Similarly, administration of the selective p110δ inhibitor IC87114 during priming prevented biased differentiation of allogeneic $CD4^+$ T cells towards an effector memory phenotype upon priming (Fig 6G-J). Of note, administration of IC87114 completely blocked Akt activation in HFD $CD4^+$ T cells, but only partially in CD mice (Fig 5A, lanes 9-11 versus 3-5). Finally, to further causally link PI3K and Akt we also treated CD WT mice with the Akt-

selective activator SC79. Similar to what we had observed *in vitro* (Fig 5K-L), this treatment led to increased effector memory differentiation to levels similar to those observed in HFD-fed animals (Fig 6G-J and S6E).

Inhibition of fatty acid oxidation prevents enhanced effector memory differentiation in saturated fatty acid-enriched diet.

Given the important role of fatty acid oxidation (FAO) in the generation of memory T cells (O'Sullivan et al., 2014), we assessed whether this metabolic pathway contributes to enhanced effector memory differentiation upon priming following saturated fatty acid-enriched diet (PED). As shown in Fig 5E-H, enrichment of dietary palmitate led to enhanced differentiation of primed $CD4^+$ T cells towards an effector memory phenotype. *In vitro*, naïve T cells increased their rate of oxidative phosphorylation (OCR: oxygen consumption rate) only in response to palmitic but not stearic acid (Fig 7A). Etomoxir is an irreversible inhibitor of carnitine palmitoyltransferase-1 (CPT-1), an upstream enzyme in the FAO cascade. We injected mice *i.p.* with etomoxir during priming in PED-fed mice and found that this treatment completely prevented biased differentiation of effector memory $CD4^+$ T cells we observed upon priming following PED (Fig 7B-E).

DISCUSSION

Chronic systemic inflammation in obesity is characterised by the secretion of Th1 cytokines as well as aberrant T cell infiltration of non-lymphoid tissue, including adipose tissue and arterial wall. Obese AT contains more Th1 lymphocytes and higher levels of IFNγ than its lean counterpart (Rocha et al., 2008). In this study we have tested the hypothesis that excess dietary saturated FA directly affects the differentiation and trafficking of $CD4^+$ T cells to non-lymphoid tissues. We report that differentiation of memory $CD4^+$ T cells primed in HFD-fed mice is biased towards a $CD44^{hi}$-$CCR7^{lo}$-$CD62L^{lo}$-$CXCR3^+$-$LFA1^+$ effector memory-like phenotype without major changes in the size of the central memory pool. These T cells display preferential trafficking to non-lymphoid, inflammatory sites as well as increased effector function following adoptive transfer. Although metabolically imbalanced DC from obese/dyslipidaemic hosts tend to support Th1/Th17 responses (Chen et al., 2014; Eguchi et al., 2012; Reynolds et al., 2012; Shamshiev et al., 2007), our data show that they play no role in determining $CD4^+$ T cell commitment to effector memory-like phenotype nor homing. The $CD4^+$ T cell developmental bias is instead mediated by direct exposure of T cells to saturated FA, i.e. palmitate, leading to enhanced activation of a PI3K p110δ/Akt-dependent pathway upon priming. Our data suggest that this pathway might involve mTORC2 leading to Akt activation but does not result in the downstream activation of mTORC1. The key role of the PI3K p110δ/Akt axis is further confirmed by our observation that selective inactivation of p110δ in HFD can re-establish homeostatic $CD4^+$ T cell responses.

A similar signalling cascade has previously been shown to direct the differentiation of $CD8^+$ effector T cells (Finlay et al., 2012; Macintyre et al., 2011), whereby high levels of Akt activation led to the down-regulation of CD62L and CCR7 expression and redirected the trafficking of effector $CD8^+$ T cells away from the secondary lymphoid tissues into the sites of inflammation. Specifically, it has been shown that downstream of TCR engagement Akt

controls transcriptional programs directing cytotoxic T cell fate but is dispensable for T cell metabolism (Macintyre et al., 2011), whilst PDK1 directly regulates mTOR and hypoxia-inducible factor 1 leading to an integrated control of metabolism and migration of $CD8^+$ T cells (Finlay et al., 2012). In addition to showing that similar signalling events underlay the differentiation of $CD4^+$ T cells, our data expand the reach of these studies from the basic mechanisms of T cell activation and effector functions control to the biased establishment of unwanted T cell responses, i.e. specific pro-inflammatory effector and migratory phenotypes, in a pathophysiologic context such as obesity. This is in line with a recent study showing the link between obesity and metabolic diseases via increased Th17 T cell differentiation (Endo et al., 2015). It has also been reported that obesity could cause impairment in the T cell memory response to secondary influenza infection, thereby affecting vaccine efficacy (Karlsson et al., 2010). As we did not observe major differences in the size of the central memory population upon priming following HFD or CD, it is possible that central memory cells are functionally impaired in obesity. In line with the above study, we observed an altered DC function following HFD.

Interestingly, our data shown in Fig 5A suggest that in physiologic conditions (CD) different upstream kinases might control the activation of Akt induced upon T cell priming as the p110δ inhibitor IC87114 did not completely block Akt phosphorylation. By contrast, in HFD mice Akt phosphorylation was completely abrogated by IC87114, indicating that the enhancement of Akt activation by dietary lipids is particularly dependent on p110δ. The molecular mechanisms of lipid exchange on the T cell membrane in physiology and during HFD remain to be fully established as well as the question as to whether FA act by altering the cell membrane lipid balance or by binding to specific receptors, as recently suggested (Eguchi et al., 2012; Haghikia et al., 2015; Wen et al., 2011). Our data showing increased membrane fluidity as well as enhanced formation of lipid rafts upon TCR engagement might provide some clues as to how excess dietary saturated FA impact on T cell responses. Similarly, our data suggest that specific mechanisms exist for palmitate sensing, which

remain to be defined. In this context, we have observed that T cell exposure to FA at the time of TCR triggering *in vitro* is not sufficient to induce the biased effector memory differentiation we observed *in vivo*, suggesting that palmitate sensing and alteration of the T cell membrane must occur prior to antigen recognition. Hence, the need to maintain naïve T cell viability over prolonged culture with or without FA and in the absence of antigen stimulation has been a major challenge in setting up in *vitro* models to study T cell differentiation following prolonged exposure to fat overload. We have partially overcome this issue by adding IL-7 to the culture of naïve T cells during incubation with or without FA prior to TCR stimulation, and this led to the results we showed in Fig 5I-J. Defining *in vitro* systems of immunization following prolonged exposure to certain nutrients would be extremely useful to test pathways involved with T cell differentiation, such as palmitate sensing.

The observation that etomoxir prevents biased differentiation of effector memory $CD4^+$ T cells upon priming following saturated fatty acid-enriched diet supports the concept that preferential utilization of FAO during T cell activation promotes effector memory $CD4^+$ T cell differentiation following HFD. AMPK-induced FAO has been shown to play an important role in the generation of memory T cells (O'Sullivan et al., 2014). Increased FAO is also a feature of HFD (Cole et al., 2011; Schrauwen et al., 2000). However, reduced AMPK activity is also observed in HFD (Lindholm et al., 2013; Liu et al., 2006), and its reactivation by metformin is known to ameliorate glucose tolerance in obesity/type II diabetes. Thus, during HFD, AMPK-induced FAO is unlikely to play a role in the biased effector memory $CD4^+$ T cell differentiation we observe. Whether and how an enhanced PI3K/Akt pathway leads to enhanced FAO remain open questions.

The biased development of pro-inflammatory effector memory $CD4^+$ T cells occurred in mice within 4-8 weeks from exposure to HFD, a time that precedes overt obesity and associated complications. This might imply a causative role of altered T cell differentiation in the pathology accompanying metabolic stress and that immune challenges occurring

naturally in individuals before the establishment of overt obesity could drive cardiovascular disease later in life.

Finally, our observation that selective PI3K p110δ and FAO inhibition can correct $CD4^+$ biased differentiation might provide targets for the therapeutic control of inflammation during metabolic stress. Likewise, our study supports the notion that by modulating metabolism we can affect immune responses, a relatively novel concept with substantial translational implications. In this regard, hints and hopes come from few recent studies, such as the report that $CD4^+$ T cells from systemic lupus erythematosus (SLE) patients exhibited enhanced glycolysis and mitochondrial metabolism that correlated with their activation status and their excessive IFNγ production was significantly reduced upon *in vitro* treatment with metformin. The same study also showed that in a number of murine lupus models the combination of metformin and 2-deoxy-glucose led to normalization of $CD4^+$ T cell metabolism and overall reversed disease biomarkers (Mehta and Chandel, 2015; Yin et al., 2015). Such studies pave the way to further research efforts in similar directions.

EXPERIMENTAL PROCEDURES

Ethical statement

Human blood was obtained from healthy donors according to ethics approval obtained from the Università degli Studi di Milano (Cholesterol and Health: Education, Control and Knowledge – Studio CHECK [SEFAP/Pr.0003] – reference number Fa-04-Feb-01). All *in vivo* experiments were conducted under the UK Home Office regulation (PPL 70/7443).

Study population

The Progressione della Lesione Intimale Carotidea (PLIC) Study (a sub-study of the CHECK Study) is a large survey of the general population living in the northern area of Milan (n=2,606; average age 66 years), (Baragetti et al., 2013; Norata et al., 2006; Norata et al., 2007), followed at the Center for the Study of Atherosclerosis, Bassini Hospital (Cinisello Balsamo, Milan, Italy). An informed consent was obtained from subjects in accordance to the Declaration of Helsinki. For all participants, information on medical histories and therapies was obtained, and Body Mass Index (BMI, Kg/m^2) and waist/hip ratio (W/H) were calculated. After an over-night fast, blood samples were collected from the antecubital vein for determination of lipid profile and glucose levels, as previously described (Ammirati et al., 2012; Baragetti et al., 2013; Norata et al., 2007). Information on total leukocytes and sub-fraction counts was available for n=1,172 subjects, representatives of the entire population in terms of age, gender distribution and clinical parameters according to the Kolmogorov-Smirnov test. This cohort was divided by BMI in accordance to the World Health Organization definition (lean for BMI < 25 Kg/m^2; overweight for 25 Kg/m^2 ≤ BMI < 30 Kg/m^2; obese for BMI ≥ 30 Kg/m^2; www.who.int).

Polychromatic flow cytometry (human studies)

Polychromatic flow cytometry (10-parameter/8-color) was performed [as previously described (Ammirati et al., 2012)] to obtain a detailed characterization of a total of n=57 subsets of circulating $CD4^+$ T cells from n=187 subjects of the PLIC Study, representative of the entire population in terms of age, gender distribution and clinical parameters according to the Kolmogorov-Smirnov test. Whole blood from each subject was collected in EDTA anticoagulated tube (BD Vacutainer). Samples were stained and fixed on the day of collection. We previously verified that there was no significant difference in the investigated marker levels in samples stained immediately after collection in comparison to samples stained up to a maximum 24-hour time interval post-sampling and stored at room temperature. In order to reduce cellular loss and analysis sampling bias in the specimen, the no wash, whole blood lyses technique was used. Briefly, for each specimen, 50 µL of a mixture of 8 antibodies (CD3/CD4/CD45RO/CD45RA/CCR7/CCR5/CXCR3/HLA-DR) was added to 100 µL of whole blood followed by 20-minute incubation in the dark at room temperature. In particular, the panel used consisted of the subsequent cellular surface markers: CD3 (Pacific Blue-labeled, clone HIT3a, BD Pharmingen), CD4 (APC-Cy7, SK3, BD Biosciences), CCR5/CD195 (PE, 2D7, BD Pharmingen), CXCR3/CD183 (FITC, 49801, R&D Systems Inc), CCR7/CD197 (PE-Cy7, 3D12, BD Pharmingen), HLA-DR (Quantum Red, HK14, Sigma-Aldrich), CD45RO (APC, UCHL1, Caltag), and CD45RA (ECD, 2H4, IOTest, Beckman Coulter). After staining, the red blood cells were lysed and fixed with the Immune-prep System (Beckman Coulter). White cells, diluted in 1 mL total volume were analyzed on a LSR II Flow Cytometer (BD Biosciences) equipped with four lasers and standard optics. The antibodies were selected to minimize spectral overlap. Furthermore, to reduce the non-specific fluorescence background and optimize the fluorescence signal, we used appropriately titrated directly conjugated monoclonal antibodies. To appropriately identify positively stained cells and differentiate them from background auto-fluorescence for gate inclusion, we used the Fluorescence Minus One strategy. Fluorescence intensity for

each signal measured was standardized using multiple peak Rainbow calibration particles (Code RCP-30-5A, Spherotech) to allow reproducible and comparable median fluorescence intensity throughout the study period, as previously described (Ammirati et al., 2010). We identified 7 principal T-cell subsets and 50 T-cell subpopulations derived by principal subsets by means of the combination of the surface markers. All data were acquired in FCS format using FACSDiva Software 5.0 (BD Biosciences). Lymphocytes were identified and electronically gated on forward and orthogonal light scatter signals. The fluorescent signals for phenotype analyses were accumulated for the gated lymphocytes. The raw data were stored electronically to a server for archiving and data processing. Data were processed and analyzed using FCS Express V3 Research edition (De Novo Software, Inc;http://www.denovosoftware.com). Cell viability was >99%, as assessed using the Molecular Probes Patented LIVE/DEAD Viability (Invitrogen), according to the manufacturer instructions.

T cell activation

In vitro: murine $CD4^+$ T cells were isolated with commercially available isolation kits (negative selection; Easysep, Invitrogen) according to manufacturer's instructions from pooled lymph nodes (inguinal, mesenteric, axillary, brachial, superficial and deep cervical, lumbar and sacral) of C57Bl/6 mice and activated with plate bound anti-CD3 (1µg/ml, ebioscience) and anti-CD28 (5µg/ml, ebioscience), and IL-2 (10ng/ml, Roche) in the presence or absence of the Akt activator SC79 (500 nM, Tocris). In alternative isolated $CD4^+$ T cells were cultured over night with IL-7 (1ng/ml, Peprotech) in the presence or absence of palmitic, linoleic or stearic acid (200µM, Sigma), followed by activation with plate bound anti-CD3 (0.5µg/ml, ebioscience) and anti-CD28 (2.5µg/ml, ebioscience).

In vivo: in Rag2KO Marilyn C57Bl/6 female mice fed CD or HFD (Test Diet; Table S2) for 8 weeks memory antigen-specific (HY-specific) $CD4^+$ T cells were generated by *i.p.* immunization with WT C57Bl/6 male splenocytes ($1.5x10^6$) for fourteen days. T cells were

then isolated from pooled lymph nodes of these mice (Fig 1A-D, 2A-G and S2A-F) and injected *i.v.* in recipients (see *in vivo* peritoneal recruitment below) or used for chemotaxis or flow cytometry.

In p110δ^{D910A} or WT C57Bl/6 mice fed HFD (or CD as control), or PED (or PCD as control; Test Diet; Table S2) for 8 weeks, memory $CD4^+$ T cells were generated by intraperitoneal immunization with CBA/BALBc splenocytes ($1.5x10^6$; allogeneic immunization) for seven days. T cells were then isolated from mesenteric lymph nodes of these mice and analysed by FACS or Western blot (Fig 2H; Fig 5A and E-H; Fig 6A-E and G-J; Fig 7). In this system, the PI3K p110δ inhibitor IC87114 (Tocris) was administered *i.p.* at a dose of 50 mg/kg daily during the 7-day immunization (Ying et al., 2012). The Akt activator SC79 (Tocris) was administered *i.p.* at a dose of 7 mg/kg daily during the 7-day immunization (Moreira et al., 2015). Etomoxir (Sigma) was administered *i.p.* at a dose of 15 mg/kg daily during the 7-day immunization (Shriver and Manchester, 2011).

In OT-II p110δ^{D910A} mice fed CD or HFD for 8 weeks, memory antigen-specific (OVA-specific) $CD4^+$ T cells were generated by intraperitoneal immunization with ovalbumin peptide (10µg, Cambridge Research Biochemicals) and Poly IC (1:1, Sigma) for seven days. T cells were then isolated from mesenteric lymph nodes of these mice (Fig 6F) and analyzed for chemotaxis.

In vivo peritoneal recruitment

In vivo activated T cells from Rag2KO Marilyn female mice were isolated from pooled lymph nodes of HFD- or CD-fed donors, labelled with CFSE (HFD; 3.3µM, Invitrogen) or PKH26 (CD; 2µM, Sigma), pooled together and intravenously injected in HFD or CD recipient male mice ($5x10^6$ cells/mouse) that had received an intraperitoneal injection with zymosan (1mg/mouse, Sigma) and IFNγ (600 U/mouse, Peprotech) 48 hours earlier. 48 hours after injection blood, peritoneal lavage, peritoneal membrane, mesenteric lymph nodes

and spleen were collected and analyzed by FACS for presence of CFSE- and PKH26-labeled T cells.

Membrane and intracellular FACS staining (murine studies)

Spleen and blood samples were lysed of their RBCs before staining. Dead cells were excluded from analysis by staining with fixable Aqua dead cell stain (Invitrogen). Isolated lymphocytes or DC were stained for surface markers; CD3, CD4, CD8, CD25, CD44, CCR7, CD62L, CXCR3, LFA1, Vβ6, CD40, CD80, CD86, MHCII, CD11c, CD19, CD14, F4/80 with fluorescently conjugated primary antibodies (1:200, ebioscience/BioLegend) at 4^{o}C for 30 minutes (37^{o}C for CCR7) in FACS buffer (PBS + 2%FCS + 0.1% sodium azide) and fixed at 4^{o}C for 30 minutes with 1% PFA in FACS buffer. For intracellular staining isolated lymphocytes were incubated in permeabilization/fixation buffer (ebioscience) at 4^{o}C for 1 hour. Samples were washed in permeabilization buffer and stained for the cytokines/chemokine IFNγ, IL4 (1:200, ebioscience/BioLegend) and CXCL10 (1:200, Stratech) with fluorescently conjugated primary antibodies at 4^{o}C for 30 minutes in permeabilization buffer. All samples were then assessed by flow cytometry using a LSR Fortessa (BD Biosciences) and FlowJo version 10 software. Dot plots were concatenated to be representative of the independent biological replicates used in each experiment.

Chemotaxis

Chemotaxis assays were performed in 5 μm transwell inlays (Corning). *In vivo* primed lymphocytes were isolated from mice fed CD or HFD for 8 weeks, suspended in migration medium (RPMI 2% FCS) and seeded in the upper transwell chamber (3x10^{5} cells/transwell). Chemokines (PeproTech) were added to the lower chamber, CXCL10 (300 ng/ml) or CCL19/21 (200 ng/ml of each chemokine). Migrated T cells were counted with a

haemocytometer 3, 6, and 24 hours after seeding, then percent of migrated cells were calculated.

Western blot

Protein lysates were prepared from; i) mesenteric lymph nodes isolated from *in vivo* primed mice fed CD or HFD for 8 weeks, ii) $CD4^+$ T lymphocytes isolated by magnetic beads (Mylteni) from lean subjects (median BMI 22.43 Kg/m^2, minimum 17.67 Kg/m^2-maximum 24.54 Kg/m^2) and obese subjects (median BMI 31.64 Kg/m^2, minimum 30.48 Kg/m^2-maximum 41.79 Kg/m^2) and iii) $CD4^+$ T lymphocytes isolated from pooled lymph nodes and activated as described above for the indicated time points. Samples were lysed in Nonidet P-40 lysis buffer (50 mM Hepes pH 8.0, 350 mM NaCl, 1% Nonidet P-40, 1 mM EDTA, 1 mM Na3VO4, 1 mM NaF, 20 mM glycerol-2-phosphate, 1 mM PMSF, 1 mM DTT, 10 µg/mL aprotinin, 10 µg/mL leupeptin, and a protease inhibitor mixture; Roche). Equivalent amounts of protein as determined by standard Bradford assay (Bio-Rad) were separated by SDS/PAGE and transferred to a Nylon membrane (GE Healthcare). Membranes were blocked for 2 hours at room temperature in 5% Milk/TBS-T (5% BSA/TBS-T for phosphorylation antibodies), incubated overnight at 4°C with primary antibodies (1:1000) and subsequently with HRP-conjugated secondary antibody (Amersham Bioscience) (1:5000). Antibodies against p-Akt (S473 and T308), Akt, p-S6 (S235/236), S6 and β-actin were purchased from Cell Signaling. Antibody against CCR7 was purchased from R&D. Density of bands was calculated relative to Akt, S6 or β-actin as shown in figures via the use of Image J software.

RNA Isolation and Reverse Transcription

RNA was isolated using commercially available kits (Qiagen) according to the manufacturer's instructions and assessed for quality and quantity using absorption measurements. Reverse transcription to cDNA was performed according to the manufacturer's instruction (Applied Biosystems).

qRT-PCR

Gene expression analysis was done using SYBR Green Supermix (Biorad) in CFX connect light cycler (Biorad), according to the manufacturer's instructions. Gene-relative expression was calculated using the ΔΔct method and normalized to a reference control (GAPDH): F 5'-GGCTCATGACCACAGTCCA-3'; R 5'-CACATTGGGGGTAGGAACAC-3'. CCR7 and CD62L primers sequences were the same as published in Finlay DK et al. J Exp Med 2012.

Mixed leukocyte reaction

In vitro: T cells were isolated from pooled lymph nodes of Rag2KO Marilyn female mice fed CD or HFD for 8 weeks and were labelled with CFSE (3.3μM) in PBS for 10 minutes at room temperature. T cells ($2x10^5$/well) were then stimulated with $CD11c^+$ DC ($7x10^4$/well) isolated from the spleen of C57Bl/6 male mice fed CD or HFD for 8 weeks. $CD11c^+$ DC were treated with mitomycin C to prevent proliferation prior to incubation with T cells. T cells were harvested 3 days later and CFSE dilution was assessed by flow cytometry (Fig 4A-B, S5A).

In vivo: T cells were isolated from pooled lymph nodes of Rag2KO Marilyn female mice, labelled with CFSE (3.3μM) in PBS for 10 minutes at room temperature and intravenously injected in C57Bl/6 recipient female mice ($5x10^6$ cells/mouse). Concurrently $CD11c^+$ DC were isolated from the spleen of C57Bl/6 male mice fed CD or HFD for 8 weeks and intraperitoneally injected in the C57Bl/6 recipient female mice (¼ spleen derived

DC/mouse). Cells were harvested from the peritoneal lavage, spleen and draining lymph nodes 5 days later and CFSE dilution was assessed by flow cytometry (Fig S5B-C).

Skin grafts

Rag2KO and Marilyn female mice fed CD or HFD for 8 weeks received a C57Bl/6 male-derived skin graft on the upper right back. Bandages were removed 7 days post-transplantation. Some Rag2KO mice were *i.v.* injected with $1x10^6$ $CD4^+$ T cells isolated from Marilyn females 9 days post-transplantation. Mice were observed for rejection for a further 3 weeks. Mice were culled 4 weeks post-transplantation.

Lipid raft staining

T cells isolated from pooled lymph nodes of C57Bl/6 mice fed CD or HFD for 8 weeks were activated as described above for 4 hours or left inactivated. Cells were stained with CTxB-FITC (8µg/ml, Sigma) and CD4-PECy7 (1:200, ebioscience) at 4^{o}C for 30 minutes in FACS buffer (PBS + 2%FCS + 0.1% sodium azide) and fixed at 4^{o}C for 30 minutes with 1% PFA in FACS buffer. Samples were assessed using Imagestream flow cytometer (Amnis) and IDEAS software. For quantitative image analysis of lipid raft aggregation, bright field and fluorescent cell images were acquired. Bright detail intensity of CTxB staining was used to quantify lipid raft aggregation. The bright detail intensity feature calculates the sum of intensity values from the brightest areas within a cell that are morphologically defined as the peak fluorescence distributions of 3 pixel radius or less. Five thousand $CD4^+$ T cells were analysed per condition.

Seahorse flux analysis

Oxidative metabolism was measured with a Seahorse XF96 Extracellular Flux Analyzer. As described before, isolated naïve $CD4^+$ T cells were cultured over night with IL-7 in the presence or absence of palmitic or stearic acid. 2 x 10^5 $CD4^+$ T cells were then seeded in a 96-well microplate in XF Assay Modified DMEM and incubated in a non-CO_2 incubator for 1 hour prior to the assay. OCR was then measured according to the manufacturer's instructions (Seahorse Bioscience).

Statistical analysis

Statistical analysis of human data was performed using SPSS v.21.0 for Windows (IBM Corporation, Chicago Illinois, USA) program. Kolmogorov-Smirnov test was performed to test whether the studied cohort was representative of the entire PLIC population in terms of age, gender distribution and clinical parameters. Shapiro-Wilk test was performed to verify the normal distribution of linear variables; median and inter-quartile range (IQR) was reported and Mann-Whitney U non parametric test was performed. Outliers detection (above and below 1.5∗IQR) was performed by use of Grubb's test. Spearman correlation coefficients (ρ) were reported for univariate correlations between linear variables. Analysis of Variances (ANOVA) test was performed to compare clinical parameters and leukocyte sub-fraction among subjects divided by BMI and then adjusted for age, gender and therapies by using Analysis of Co-Variances (ANCOVA). For all analysis, statistically relevant differences were considered for p values < 0.05.

For murine studies, data are expressed as mean ± s.e.m. Two-tailed Student's t-test was used to compare 2 groups with parametric data distribution. For multiple comparison analysis, 1-, 2- or 3-way ANOVA was used, unless otherwise specified (Fig 1E). In all case, a p-value of less than 5% was considered to be significant.

AUTHOR CONTRIBUTIONS

Conceived and designed the experiments: CM, JS, GDN and FMM-B. Performed the experiments: CM, JS, D Cucchi, D Coe, FB, AB, GC, D Caruso and NM. Analyzed the data: CM, JS, D Coe, HF, FB, AB, GC, D Caruso, NM, EA and GDN. Contributed reagents/materials/analysis tools: MPL, KO, ALC, EA. Wrote the paper: CM, JS, GDN and FMM-B.

AKNOWLEDGEMENTS

This work was supported by the British Heart Foundation (Fellowship FS/12/38/29640 and Project Grant PG/15/105/31906 to CM) and the Fondazione Cariplo (a Project Grant to CM and GDN), and forms part of the research themes contributing to the translational research portfolio of Barts and the London Cardiovascular Biomedical Research Unit, which is supported and funded by the National Institutes of Health Research. D Cucchi was supported in part by a Fellowship from the Istituto Pasteur, Fondazione Cenci-Bolognetti. GDN was supported by the Telethon Foundation (GGP13002) and the Italian Ministero della Salute (WFR GR-2011-02346974).

REFERENCES

Ammirati, E., Cianflone, D., Banfi, M., Vecchio, V., Palini, A., De Metrio, M., Marenzi, G., Panciroli, C., Tumminello, G., Anzuini, A.*, et al.* (2010). Circulating CD4+CD25hiCD127lo regulatory T-Cell levels do not reflect the extent or severity of carotid and coronary atherosclerosis. Arteriosclerosis, thrombosis, and vascular biology *30*, 1832-1841.

Ammirati, E., Cianflone, D., Vecchio, V., Banfi, M., Vermi, A.C., De Metrio, M., Grigore, L., Pellegatta, F., Pirillo, A., Garlaschelli, K.*, et al.* (2012). Effector Memory T cells Are Associated With Atherosclerosis in Humans and Animal Models. Journal of the American Heart Association *1*, 27-41.

Baragetti, A., Norata, G.D., Sarcina, C., Rastelli, F., Grigore, L., Garlaschelli, K., Uboldi, P., Baragetti, I., Pozzi, C., and Catapano, A.L. (2013). High density lipoprotein cholesterol levels are an independent predictor of the progression of chronic kidney disease. Journal of internal medicine *274*, 252-262.

Bjorndal, B., Burri, L., Staalesen, V., Skorve, J., and Berge, R.K. (2011). Different adipose depots: their role in the development of metabolic syndrome and mitochondrial response to hypolipidemic agents. Journal of obesity *2011*, 490650.

Cermenati, G., Audano, M., Giatti, S., Carozzi, V., Porretta-Serapiglia, C., Pettinato, E., Ferri, C., D'Antonio, M., De Fabiani, E., Crestani, M.*, et al.* (2015). Lack of sterol regulatory element binding factor-1c imposes glial Fatty Acid utilization leading to peripheral neuropathy. Cell metabolism *21*, 571-583.

Chen, Y., Demir, Y., Valujskikh, A., and Heeger, P.S. (2003). The male minor transplantation antigen preferentially activates recipient CD4+ T cells through the indirect presentation pathway in vivo. Journal of immunology (Baltimore, Md. : 1950) *171*, 6510-6518.

Chen, Y., Tian, J., Tian, X., Tang, X., Rui, K., Tong, J., Lu, L., Xu, H., and Wang, S. (2014). Adipose tissue dendritic cells enhances inflammation by prompting the generation of Th17 cells. PloS one *9*, e92450.

Cildir, G., Akincilar, S.C., and Tergaonkar, V. (2013). Chronic adipose tissue inflammation: all immune cells on the stage. Trends in molecular medicine *19*, 487-500.

Cole, M.A., Murray, A.J., Cochlin, L.E., Heather, L.C., McAleese, S., Knight, N.S., Sutton, E., Jamil, A.A., Parassol, N., and Clarke, K. (2011). A high fat diet increases mitochondrial fatty acid oxidation and uncoupling to decrease efficiency in rat heart. Basic research in cardiology *106*, 447-457.

Eguchi, K., Manabe, I., Oishi-Tanaka, Y., Ohsugi, M., Kono, N., Ogata, F., Yagi, N., Ohto, U., Kimoto, M., Miyake, K.*, et al.* (2012). Saturated fatty acid and TLR signaling link beta cell dysfunction and islet inflammation. Cell metabolism *15*, 518-533.

Endo, Y., Asou, H.K., Matsugae, N., Hirahara, K., Shinoda, K., Tumes, D.J., Tokuyama, H., Yokote, K., and Nakayama, T. (2015). Obesity Drives Th17 Cell Differentiation by Inducing the Lipid Metabolic Kinase, ACC1. Cell reports *12*, 1042-1055.

Faulds, M.H., and Dahlman-Wright, K. (2012). Metabolic diseases and cancer risk. Current opinion in oncology *24*, 58-61.

Finlay, D.K., Rosenzweig, E., Sinclair, L.V., Feijoo-Carnero, C., Hukelmann, J.L., Rolf, J., Panteleyev, A.A., Okkenhaug, K., and Cantrell, D.A. (2012). PDK1 regulation of mTOR and hypoxia-inducible factor 1 integrate metabolism and migration of CD8+ T cells. The Journal of experimental medicine *209*, 2441-2453.

Fu, H., Kishore, M., Gittens, B., Wang, G., Coe, D., Komarowska, I., Infante, E., Ridley, A.J., Cooper, D., Perretti, M., and Marelli-Berg, F.M. (2014). Self-recognition of the endothelium enables regulatory T-cell trafficking and defines the kinetics of immune regulation. Nature communications *5*, 3436.

Gerriets, V.A., and Rathmell, J.C. (2012). Metabolic pathways in T cell fate and function. Trends in immunology *33*, 168-173.

Gupta, S., Pablo, A.M., Jiang, X., Wang, N., Tall, A.R., and Schindler, C. (1997). IFN-gamma potentiates atherosclerosis in ApoE knock-out mice. The Journal of clinical investigation *99*, 2752-2761.

Haghikia, A., Jorg, S., Duscha, A., Berg, J., Manzel, A., Waschbisch, A., Hammer, A., Lee, D.H., May, C., Wilck, N.*, et al.* (2015). Dietary Fatty Acids Directly Impact Central Nervous System Autoimmunity via the Small Intestine. Immunity *43*, 817-829.

Hamann, A., Klugewitz, K., Austrup, F., and Jablonski-Westrich, D. (2000). Activation induces rapid and profound alterations in the trafficking of T cells. European journal of immunology *30*, 3207-3218.

Karlsson, E.A., Sheridan, P.A., and Beck, M.A. (2010). Diet-induced obesity impairs the T cell memory response to influenza virus infection. Journal of immunology (Baltimore, Md. : 1950) *184*, 3127-3133.

Lantz, O., Grandjean, I., Matzinger, P., and Di Santo, J.P. (2000). Gamma chain required for naive CD4+ T cell survival but not for antigen proliferation. Nature immunology *1*, 54-58.

Larbi, A., Franceschi, C., Mazzatti, D., Solana, R., Wikby, A., and Pawelec, G. (2008). Aging of the immune system as a prognostic factor for human longevity. Physiology (Bethesda, Md.) *23*, 64-74.

Lindholm, C.R., Ertel, R.L., Bauwens, J.D., Schmuck, E.G., Mulligan, J.D., and Saupe, K.W. (2013). A high-fat diet decreases AMPK activity in multiple tissues in the absence of hyperglycemia or systemic inflammation in rats. Journal of physiology and biochemistry *69*, 165-175.

Liu, Y., Wan, Q., Guan, Q., Gao, L., and Zhao, J. (2006). High-fat diet feeding impairs both the expression and activity of AMPKa in rats' skeletal muscle. Biochemical and biophysical research communications *339*, 701-707.

Macintyre, A.N., Finlay, D., Preston, G., Sinclair, L.V., Waugh, C.M., Tamas, P., Feijoo, C., Okkenhaug, K., and Cantrell, D.A. (2011). Protein kinase B controls transcriptional programs that direct cytotoxic T cell fate but is dispensable for T cell metabolism. Immunity *34*, 224-236.

Mathis, D., and Shoelson, S.E. (2011). Immunometabolism: an emerging frontier. Nature reviews. Immunology *11*, 81.

Mauro, C., and Marelli-Berg, F.M. (2012). T cell immunity and cardiovascular metabolic disorders: does metabolism fuel inflammation? Frontiers in immunology *3*, 173.

Mehta, M.M., and Chandel, N.S. (2015). Targeting metabolism for lupus therapy. Science translational medicine *7*, 274fs275.

Molinero, L.L., Yin, D., Lei, Y.M., Chen, L., Wang, Y., Chong, A.S., and Alegre, M.L. (2016). High-Fat Diet-Induced Obesity Enhances Allograft Rejection. Transplantation *100*, 1015-1021.

Moreira, J.B., Wohlwend, M., Alves, M.N., Wisloff, U., and Bye, A. (2015). A small molecule activator of AKT does not reduce ischemic injury of the rat heart. Journal of translational medicine *13*, 76.

Norata, G.D., Caligiuri, G., Chavakis, T., Matarese, G., Netea, M.G., Nicoletti, A., O'Neill, L.A., and Marelli-Berg, F.M. (2015). The Cellular and Molecular Basis of Translational Immunometabolism. Immunity *43*, 421-434.

Norata, G.D., Garlaschelli, K., Ongari, M., Raselli, S., Grigore, L., and Catapano, A.L. (2006). Effects of fractalkine receptor variants on common carotid artery intima-media thickness. Stroke; a journal of cerebral circulation *37*, 1558-1561.

Norata, G.D., Raselli, S., Grigore, L., Garlaschelli, K., Dozio, E., Magni, P., and Catapano, A.L. (2007). Leptin:adiponectin ratio is an independent predictor of intima media thickness of the common carotid artery. Stroke; a journal of cerebral circulation *38*, 2844-2846.

O'Sullivan, D., van der Windt, G.J., Huang, S.C., Curtis, J.D., Chang, C.H., Buck, M.D., Qiu, J., Smith, A.M., Lam, W.Y., DiPlato, L.M.*, et al.* (2014). Memory CD8(+) T cells use cell-intrinsic lipolysis to support the metabolic programming necessary for development. Immunity *41*, 75-88.

Okkenhaug, K., Bilancio, A., Farjot, G., Priddle, H., Sancho, S., Peskett, E., Pearce, W., Meek, S.E., Salpekar, A., Waterfield, M.D.*, et al.* (2002). Impaired B and T cell antigen receptor signaling in p110delta PI 3-kinase mutant mice. Science (New York, N.Y.) *297*, 1031-1034.

Reynolds, C.M., McGillicuddy, F.C., Harford, K.A., Finucane, O.M., Mills, K.H., and Roche, H.M. (2012). Dietary saturated fatty acids prime the NLRP3 inflammasome via TLR4 in dendritic cells-implications for diet-induced insulin resistance. Molecular nutrition & food research *56*, 1212-1222.

Robertson, N.J., Chai, J.G., Millrain, M., Scott, D., Hashim, F., Manktelow, E., Lemonnier, F., Simpson, E., and Dyson, J. (2007). Natural regulation of immunity to minor histocompatibility antigens. Journal of immunology (Baltimore, Md. : 1950) *178*, 3558-3565.

Rocha, V.Z., Folco, E.J., Ozdemir, C., Sheikine, Y., Christen, T., Sukhova, G.K., Tang, E.H., Bittencourt, M.S., Santos, R.D., Luster, A.D.*, et al.* (2014). CXCR3 controls T-cell accumulation in fat inflammation. Arteriosclerosis, thrombosis, and vascular biology *34*, 1374-1381.

Rocha, V.Z., Folco, E.J., Sukhova, G., Shimizu, K., Gotsman, I., Vernon, A.H., and Libby, P. (2008). Interferon-gamma, a Th1 cytokine, regulates fat inflammation: a role for adaptive immunity in obesity. Circulation research *103*, 467-476.

Rothney, M.P., Xia, Y., Wacker, W.K., Martin, F.P., Beaumont, M., Rezzi, S., Giusti, V., and Ergun, D.L. (2013). Precision of a new tool to measure visceral adipose tissue (VAT) using dual-energy X-Ray absorptiometry (DXA). Obesity (Silver Spring, Md.) *21*, E134-136.

Schrauwen, P., Wagenmakers, A.J., van Marken Lichtenbelt, W.D., Saris, W.H., and Westerterp, K.R. (2000). Increase in fat oxidation on a high-fat diet is accompanied by an increase in triglyceride-derived fatty acid oxidation. Diabetes *49*, 640-646.

Shamshiev, A.T., Ampenberger, F., Ernst, B., Rohrer, L., Marsland, B.J., and Kopf, M. (2007). Dyslipidemia inhibits Toll-like receptor-induced activation of CD8alpha-negative dendritic cells and protective Th1 type immunity. The Journal of experimental medicine *204*, 441-452.

Shaw, A.C., Joshi, S., Greenwood, H., Panda, A., and Lord, J.M. (2010). Aging of the innate immune system. Current opinion in immunology *22*, 507-513.

Shriver, L.P., and Manchester, M. (2011). Inhibition of fatty acid metabolism ameliorates disease activity in an animal model of multiple sclerosis. Scientific reports *1*, 79.

Swamy, M., Beck-Garcia, K., Beck-Garcia, E., Hartl, F.A., Morath, A., Yousefi, O.S., Dopfer, E.P., Molnar, E., Schulze, A.K., Blanco, R.*, et al.* (2016). A Cholesterol-Based Allostery Model of T Cell Receptor Phosphorylation. Immunity *44*, 1091-1101.

Veillard, N.R., Steffens, S., Pelli, G., Lu, B., Kwak, B.R., Gerard, C., Charo, I.F., and Mach, F. (2005). Differential influence of chemokine receptors CCR2 and CXCR3 in development of atherosclerosis in vivo. Circulation *112*, 870-878.

Viola, A., Schroeder, S., Sakakibara, Y., and Lanzavecchia, A. (1999). T lymphocyte costimulation mediated by reorganization of membrane microdomains. Science (New York, N.Y.) *283*, 680-682.

Wen, H., Gris, D., Lei, Y., Jha, S., Zhang, L., Huang, M.T., Brickey, W.J., and Ting, J.P. (2011). Fatty acid-induced NLRP3-ASC inflammasome activation interferes with insulin signaling. Nature immunology *12*, 408-415.

Yin, Y., Choi, S.C., Xu, Z., Perry, D.J., Seay, H., Croker, B.P., Sobel, E.S., Brusko, T.M., and Morel, L. (2015). Normalization of CD4+ T cell metabolism reverses lupus. Science translational medicine *7*, 274ra218.

Ying, H., Fu, H., Rose, M.L., McCormack, A.M., Sarathchandra, P., Okkenhaug, K., and Marelli-Berg, F.M. (2012). Genetic or pharmaceutical blockade of phosphoinositide 3-kinase p110delta prevents chronic rejection of heart allografts. PloS one *7*, e32892.

FIGURE LEGENDS

Figure 1. Priming following HFD induces differentiation of a CD4$^+$ T cell population that readily migrates to inflamed, non-lymphoid tissues independent of the metabolic status of the host. *In vivo*-primed CD4$^+$ T cells isolated from pooled lymph nodes of HFD or CD Marilyn female donor mice, fluorescently labelled with CFSE or PKH26 respectively, in different tissue compartments (as described) of HFD or CD C57Bl/6 male recipient mice 48h post *i.v.* injection of donor cells. Male recipients were previously *i.p.* injected with zymosan (1mg/mouse) and IFNγ (600U/mouse). **(A)** Dot plots and quantification of donor cells in the blood circulation of CD recipient mice; 2hr, 24hr and 48hr post *i.v.* injection of donor cells. **(B-D)** Dot plots and quantification of the localisation of donor cells, fluorescently labelled with CFSE (HFD) or PKH26 (CD) in the peritoneal cavity **(B)**, mesenteric lymph nodes **(C)** and spleen **(D)** of HFD or CD recipient mice. **(E)** Survival curve of C57Bl/6 male skin grafts on HFD or CD Marilyn female recipient mice up to 28 days post-transplantation. **(A-D)** n=4-6 independent recipients. **(E)** n=7 HFD, n=9 CD independent recipients. Values denote mean ± s.e.m. *P<0.05; **P<0.01; ***P<0.001. **(E)** Mantel-Cox test, *P<0.05.

Figure 2. HFD-induced metabolic stress promotes the differentiation of primed CD4$^+$ T cells to a CXCR3$^+$-LFA1$^+$ effector memory-like phenotype in mice. (A-F) Cell surface staining of CD25, CD44, CCR7, CD62L, CXCR3 and LFA1 in *in vivo*-primed CD4$^+$ T cells isolated from pooled lymph nodes of the HFD or CD Marilyn female donor mice used in Fig 1A-D (absolute numbers). **(G)** *Ex vivo* chemotaxis (3hr, 6hr and 24hr time points) of *in vivo*-primed CD4$^+$ T cells isolated from pooled lymph nodes of the HFD or CD Marilyn female donor mice used in Fig 1A-D in response to CXCL10 (300ng/ml), CCL19/21 (200ng/ml of each chemokine) or media only. **(H-I)** Intracellular staining of IFNγ and IL4 in *in vivo*-primed CD4$^+$ T cells isolated from mesenteric lymph nodes of HFD or CD mice. **(A-F)** n=4-6

independent donors. **(G)** n=3 independent donors (each donor was tested in duplicate). **(H-I)** n=5 independent mice. Values denote mean ± s.e.m. *P<0.05; **P<0.01; ***P<0.001.

Figure 3. Obesity and body fat distribution in humans positively associates with an increase in CXCR3$^+$ effector memory T cells. (A-D) Number of total lymphocytes **(A)** and % of helper, naïve and effector memory T cells **(B-D)** purified from the peripheral blood of lean, over-weight and obese subjects stratified according to BMI. **(E)** % of effector memory T cells purified from the peripheral blood of obese subjects stratified according to BMI either <35 or ≥35. **(F-H)** Correlation of naïve, effector memory and CXCR3$^+$ T cells with android/gynoid ratio. **(A)** n=1,172. **(B-D and F-H)** n=187. **(E)** n=21 BMI <35, n=5 BMI≥35. ANCOVA, *P<0.05.

Figure 4. Antigen presentation by DC from metabolically stressed donors does not affect T cell differentiation to a pro-inflammatory effector memory-like phenotype. (A) Dot plots and quantification of *in vitro* proliferation of CFSE-labelled CD4$^+$ T cells isolated from pooled lymph nodes of HFD or CD Marilyn female mice incubated for 3 days with CD11c$^+$ DC isolated from the spleen of HFD or CD C57Bl/6 male mice. Undivided and 4th division populations are quantified by dilution of the CFSE-label. **(B)** Cell surface staining of CD44, CCR7, CD62L and CXCR3 in the undivided population of CFSE-labelled CD4$^+$ T cells shown in A. **(C)** Cell surface staining of CD40, CD80 and CD86 in CD11c$^+$ DC used in A. **(A-B)** n=3 independent mice (each mouse was tested in triplicate). **(C)** n=3 independent mice. Values denote mean ± s.e.m. **P<0.01; ***P<0.001.

Figure 5. Direct exposure of CD4$^+$ T cells to saturated FA causes enhanced activation of a PI3K p110δ/Akt-dependent pathway upon priming. (A) Levels and densitometric quantification of p-Akt (S473), Akt, p-S6 (S235/236) and β-actin protein expression in *in vivo*-primed CD4$^+$ T cells isolated from mesenteric lymph nodes of CD and HFD mice *i.p.* injected

with the PI3K inhibitor IC87114 or left untreated. **(B)** Levels and densitometric quantification of p-Akt (S473) and Akt protein expression in $CD4^+$ T cells purified from the peripheral blood of lean and obese human subjects. **(C)** Membrane fluidity index in *in vivo*-primed $CD4^+$ T cells isolated from mesenteric lymph nodes of CD and HFD mice, calculated as the ratio of oleic acid (C18:1) to linoleic acid (C18:2). **(D)** Cell surface staining of CTxB in *in vitro* activated (Act) $CD4^+$ T cells isolated from the lymph nodes of CD and HFD mice. Quantification of aggregation of CTxB is measured by Bright Detail Intensity of the signal. **(E-H)** Cell surface staining of CD44, CCR7, CD62L, CXCR3 and LFA1 in *in vivo*-primed $CD4^+$ T cells isolated from mesenteric lymph nodes of PED and PCD mice. **(I-J)** Protein levels and densitometric quantification of p-Akt (S473), Akt, p-S6 (S235/236) and S6 protein expression **(I)**, and gene expression of CCR7 and CD62L **(J)** in $CD4^+$ T cells isolated from pooled lymph nodes of mice and cultured over night with IL-7 (1ng/ml) in the presence or absence of palmitic, linoleic or stearic acid (200µM), followed by activation with plate bound anti-CD3 (0.5µg/ml) and anti-CD28 (2.5µg/ml) for the indicated time points. **(K-L)** Levels of CCR7 and CD62L gene expression **(K)** and CCR7 protein **(L)** in $CD4^+$ T cells isolated from pooled lymph nodes of mice, then activated with plate bound anti-CD3 (0.5µg/ml) and anti-CD28 (2.5µg/ml) for the indicated time points in the presence or absence of the Akt activator SC79 (500 nM). **(A-B)** Each lane shows data from independent mouse/human samples. **(C-H)** n=3-6 independent mice. **(I)** Representative data of n=3 independent mice. **(J-L)** 3-6 pooled mice. Values denote mean ± s.e.m. *P<0.05; **P<0.01; *** P<0.001.

Figure 6. The PI3K/Akt pathway is key for the differentiation of $CXCR3^+$ effector memory T cells. **(A-D)** Cell surface staining of CD44, CCR7, CD62L, CXCR3 and LFA1 in *in vivo*-primed $CD4^+$ T cells isolated from mesenteric lymph nodes of HFD $P110\delta^{D910A}$ or WT C57Bl/6 mice. **(E)** Levels and densitometric quantification of p-Akt (S473), Akt, p-S6 (S235/236) and S6 protein expression in *in vivo*-primed $CD4^+$ T cells from A-D. **(F)** *Ex vivo* chemotaxis (3hr, 6hr and 24hr time points) of *in vivo*-primed $CD4^+$ T cells isolated from

mesenteric lymph nodes of HFD or CD OT-II P110δ^{D910A} mice in response to CXCL10 (300ng/ml), CCL19/21 (200ng/ml of each chemokine) or media only. **(G-J)** Cell surface staining of CD44, CCR7, CD62L, CXCR3 and LFA1 in *in vivo*-primed $CD4^+$ T cells isolated from mesenteric lymph nodes of CD and HFD mice *i.p.* injected with the PI3K inhibitor IC87114, the Akt activator SC79 or left untreated. **(A-E, G-J)** n=5 independent mice. **(F)** n=4 independent mice (each mouse was tested in duplicate). Values denote mean ± s.e.m. *P<0.05; **P<0.01; *** P<0.001.

Figure 7. Inhibition of FAO prevents enhanced effector memory differentiation in saturated fatty acid-enriched diet. (A) OCR of naïve $CD4^+$ T cells isolated from pooled lymph nodes of mice and cultured over night with IL-7 (1ng/ml) in the presence or absence of palmitic or stearic acid (200µM). **(B-E)** Cell surface staining of CD44, CCR7, CD62L, CXCR3 and LFA1 in *in vivo*-primed $CD4^+$ T cells isolated from mesenteric lymph nodes of PED or PCD mice *i.p.* injected with etomoxir or left untreated. **(A)** 6 pooled mice tested in 6-10 replicates per treatment. **(B-E)** n=5 independent mice. Values denote mean ± s.e.m. *P<0.05; **P<0.01.

Fig 1

Click here to download Figure Figure1 300dpi.tif

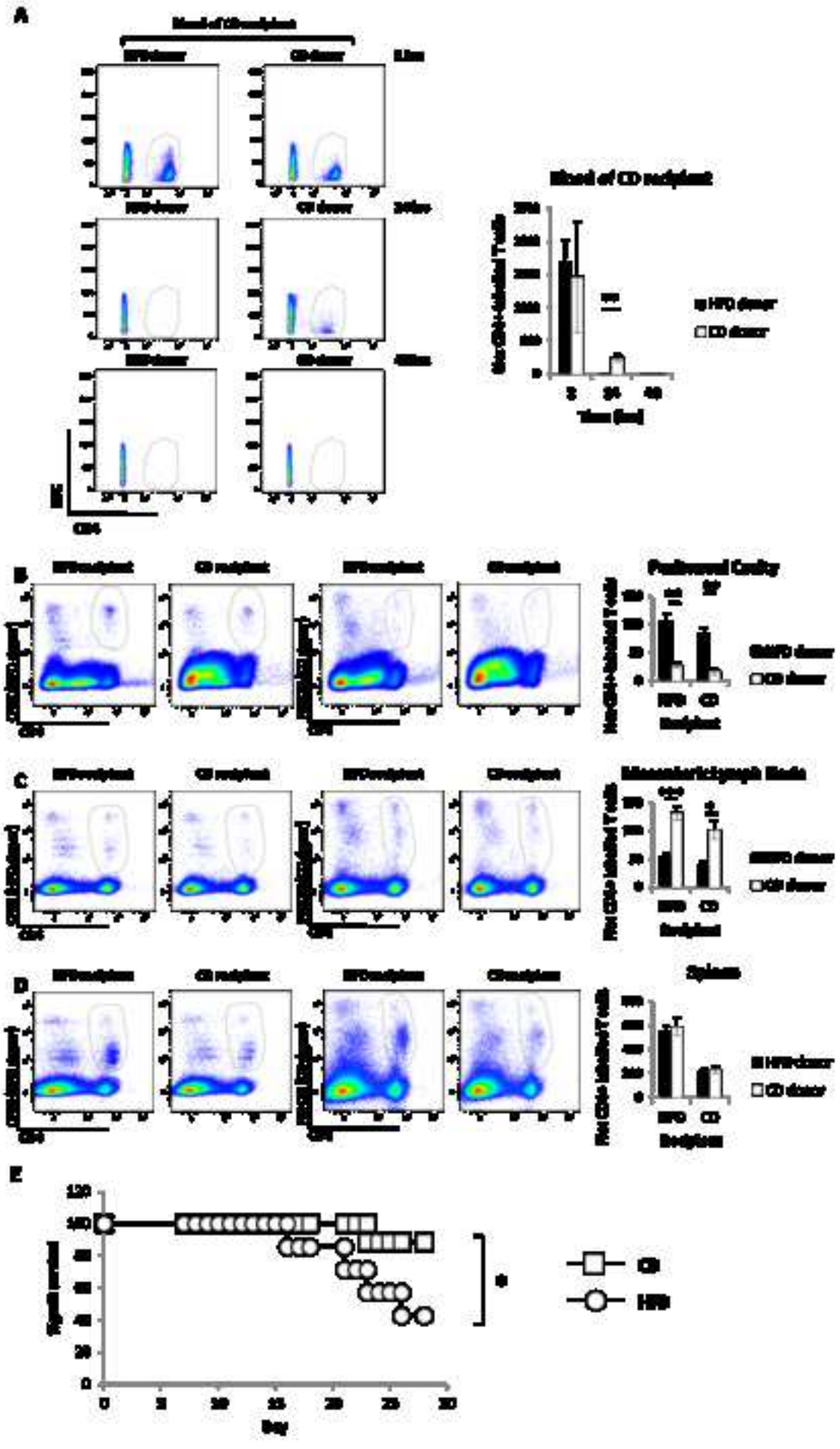

Fig 2

Click here to download Figure Figure2 300dpi.tif

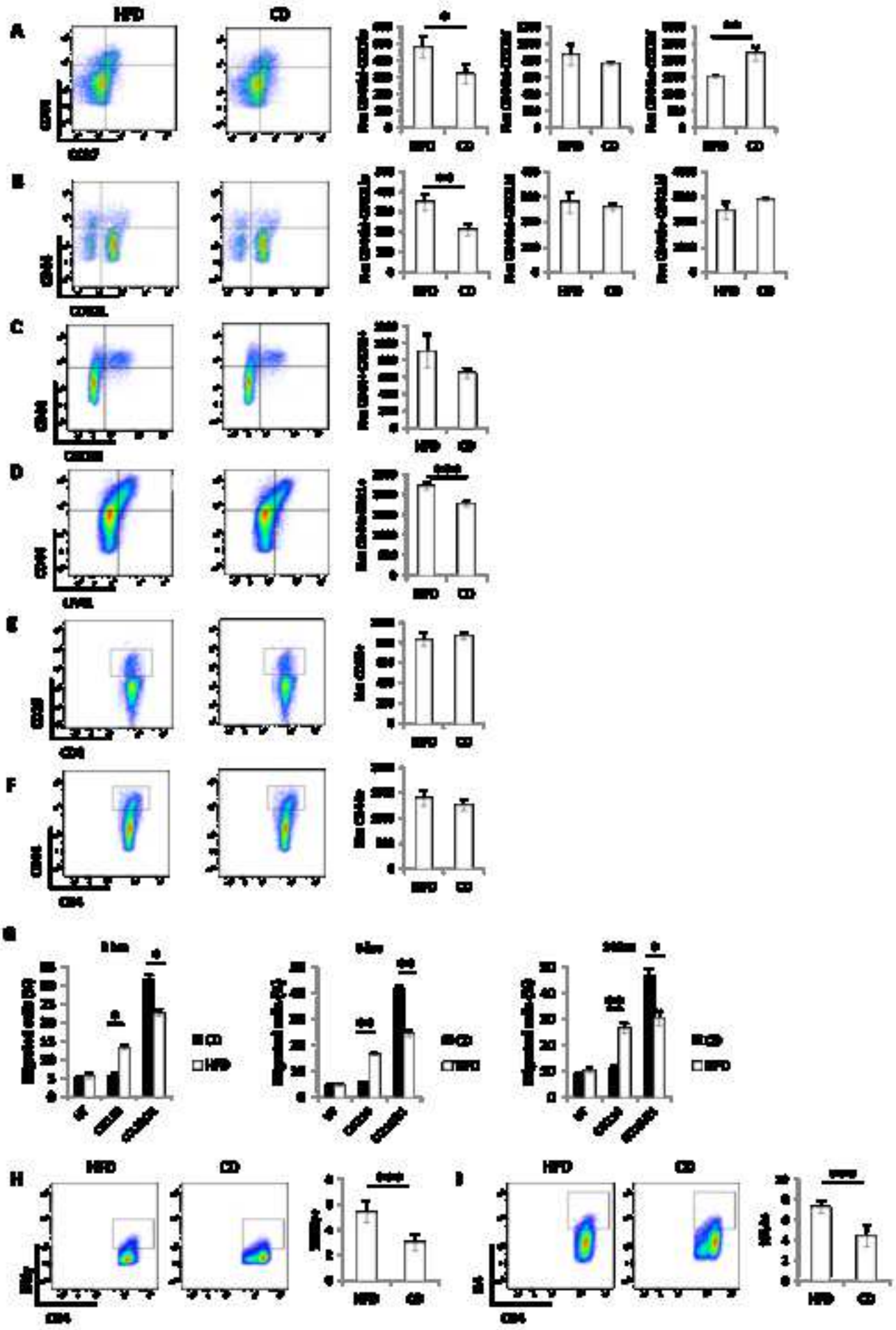

Fig 3

Click here to download Figure Figure3 500dpi.tif

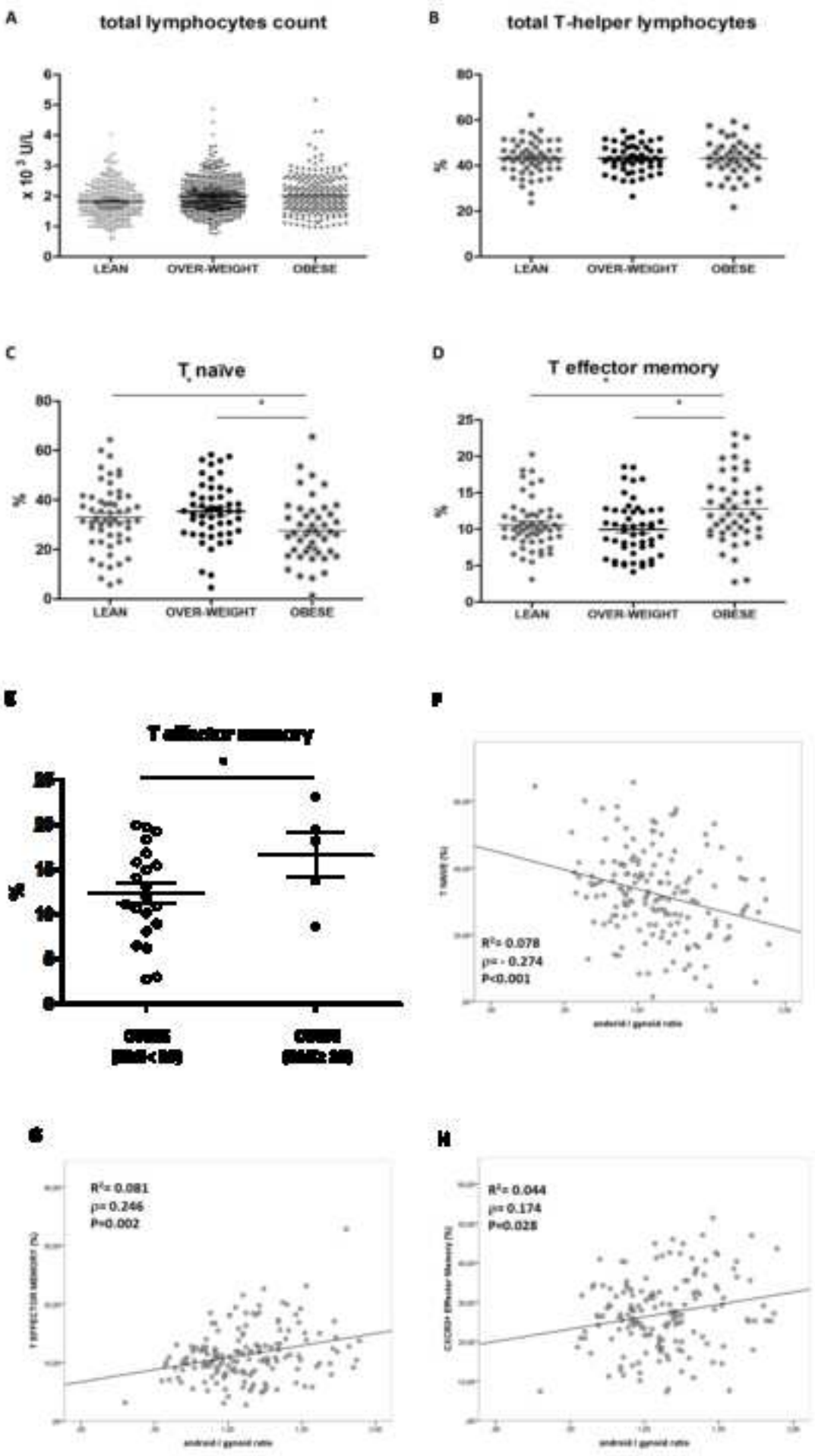

Fig 4

Click here to download Figure Figure4 300dpi.tif

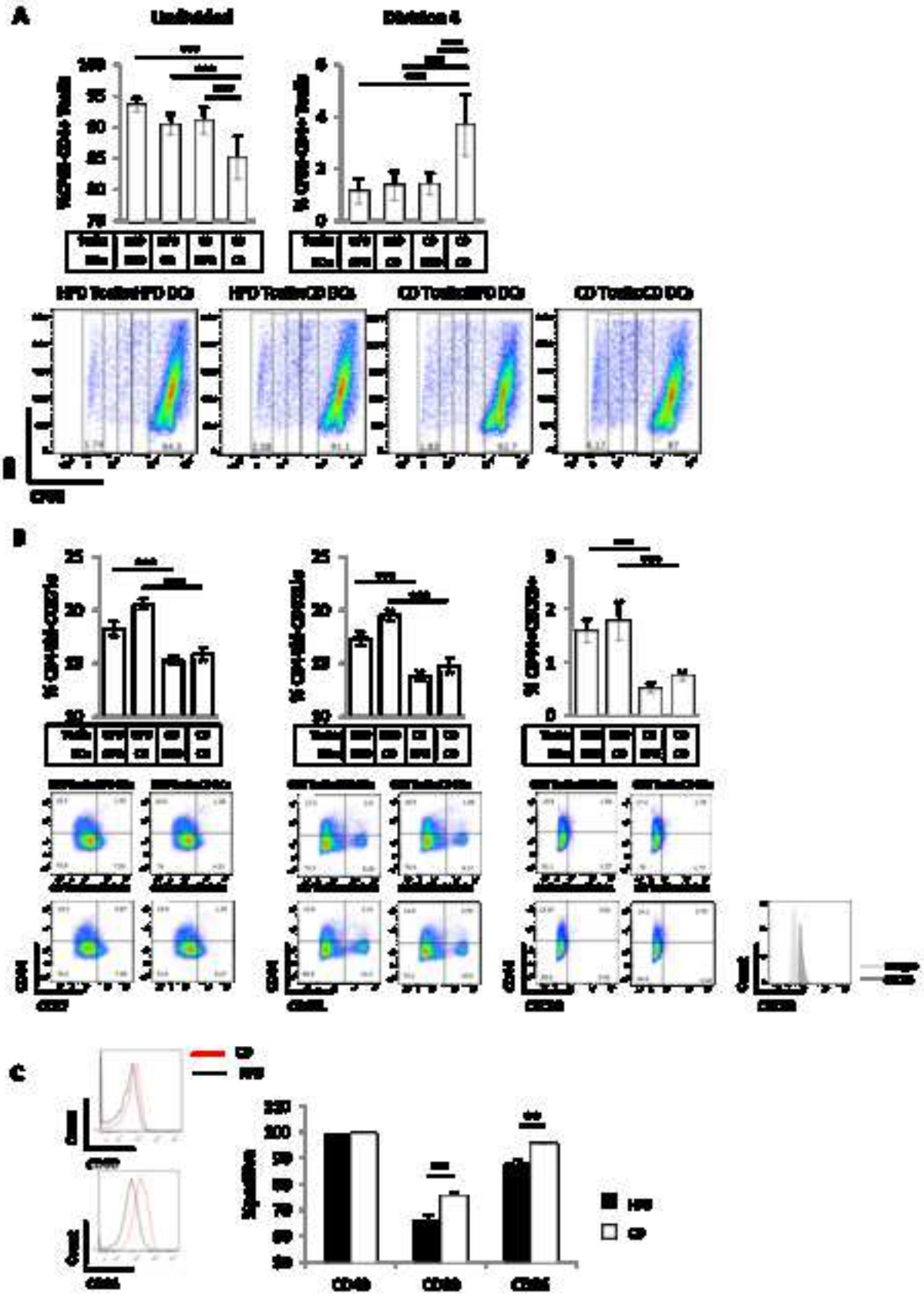

Fig 5

Click here to download Figure Figure5 300dpi.tif

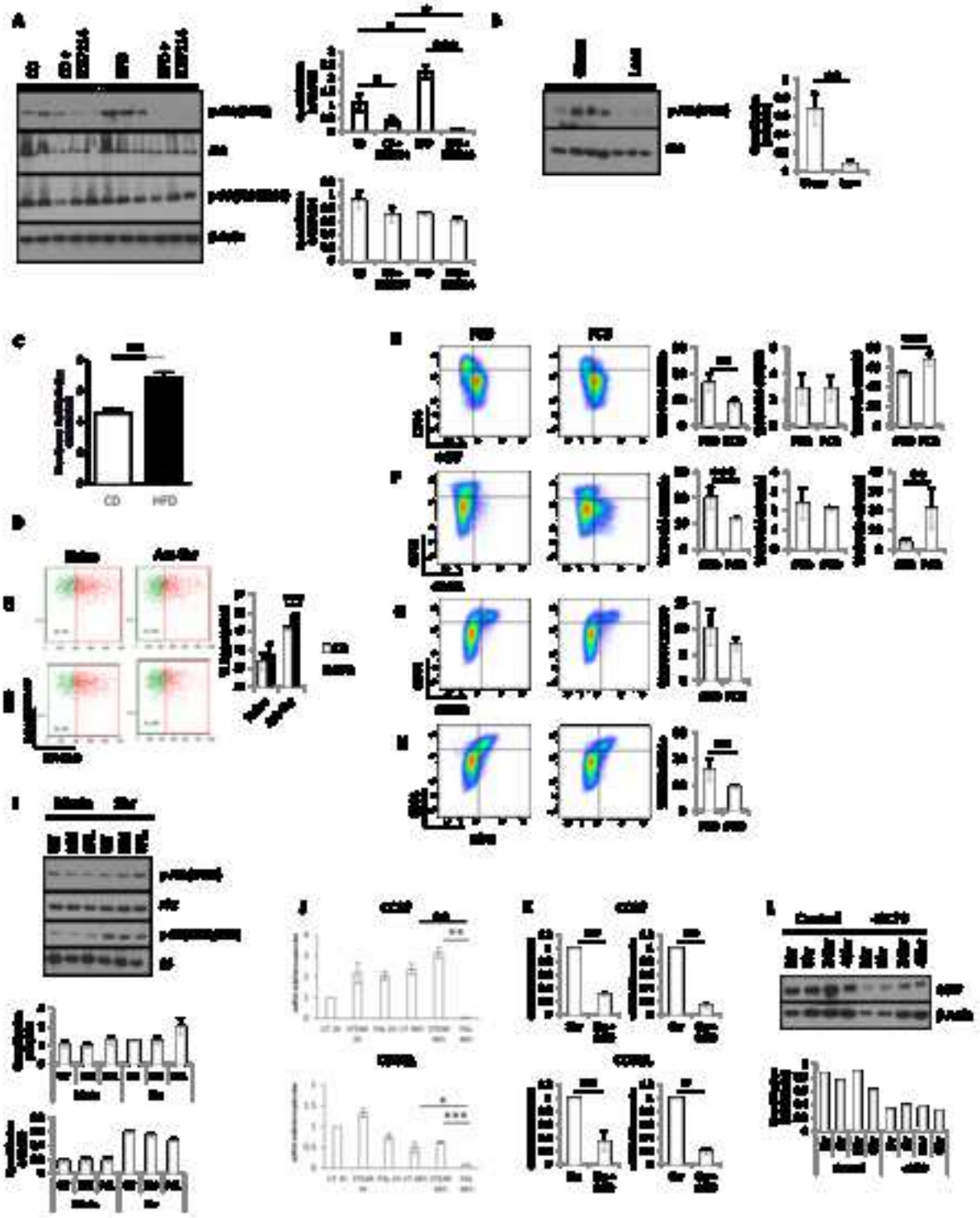

Fig 6

Click here to download Figure Figure6 300dpi.tif

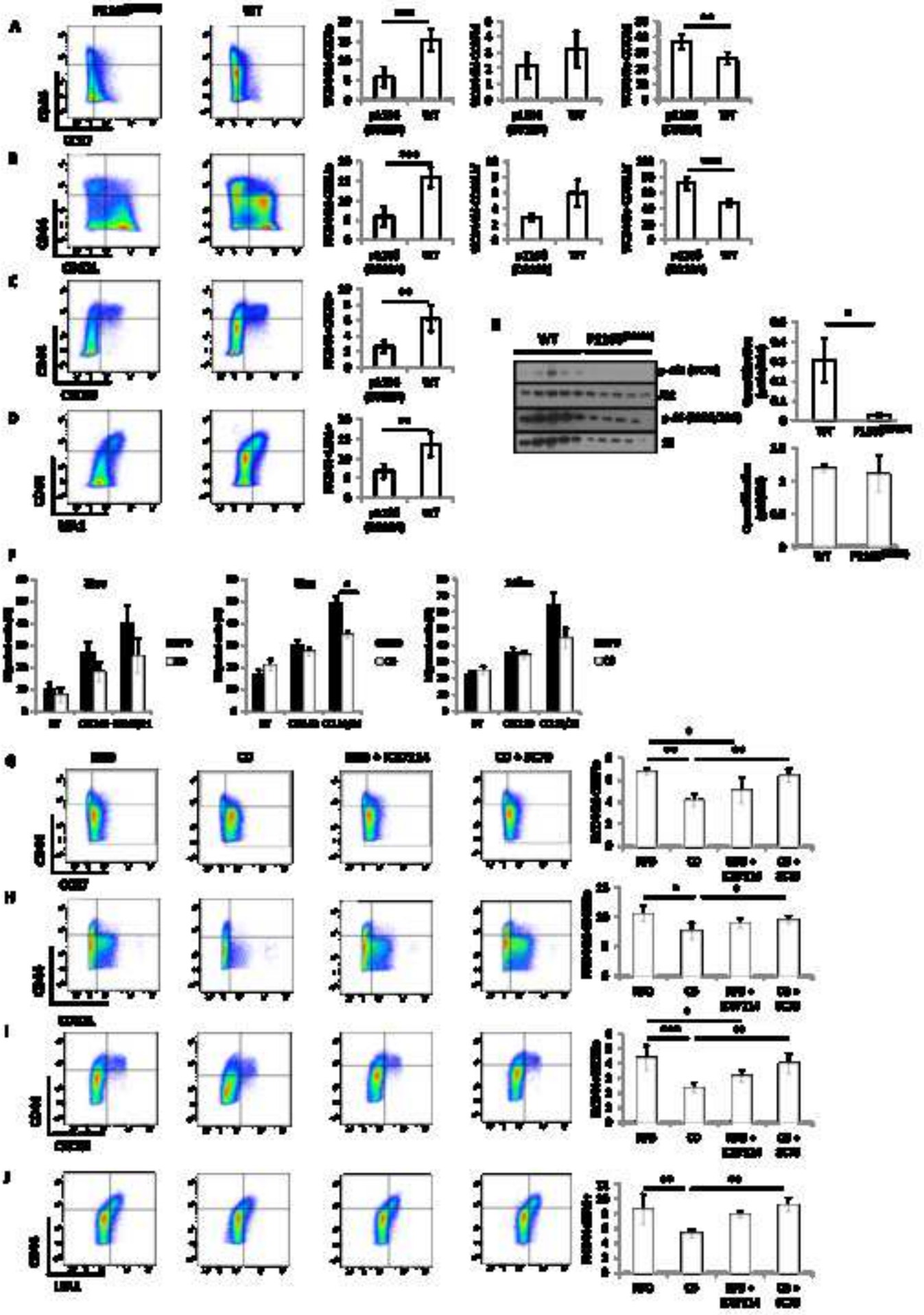

Fig 7

Click here to download Figure Figure7 300dpi.tif

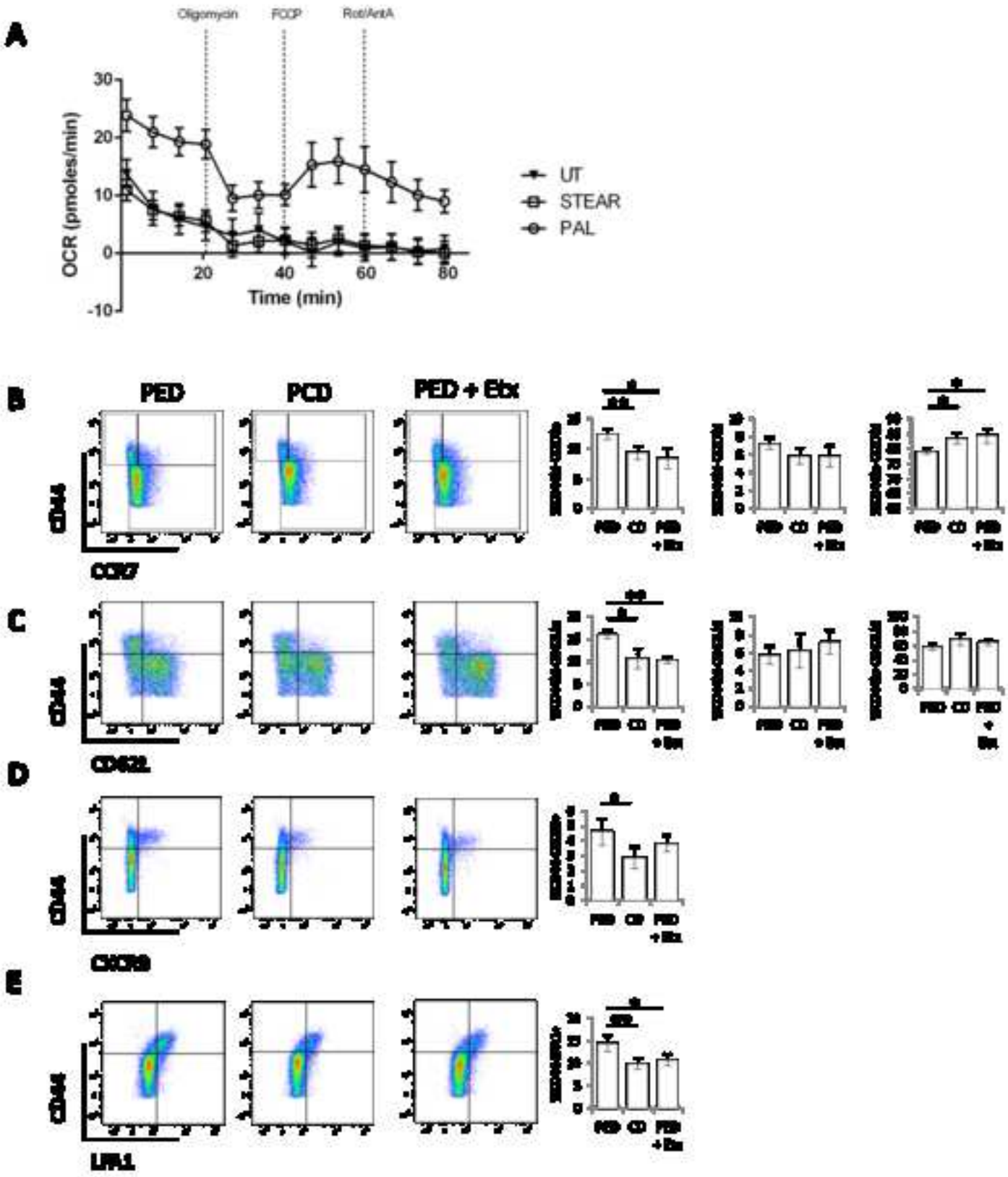

Figure S1

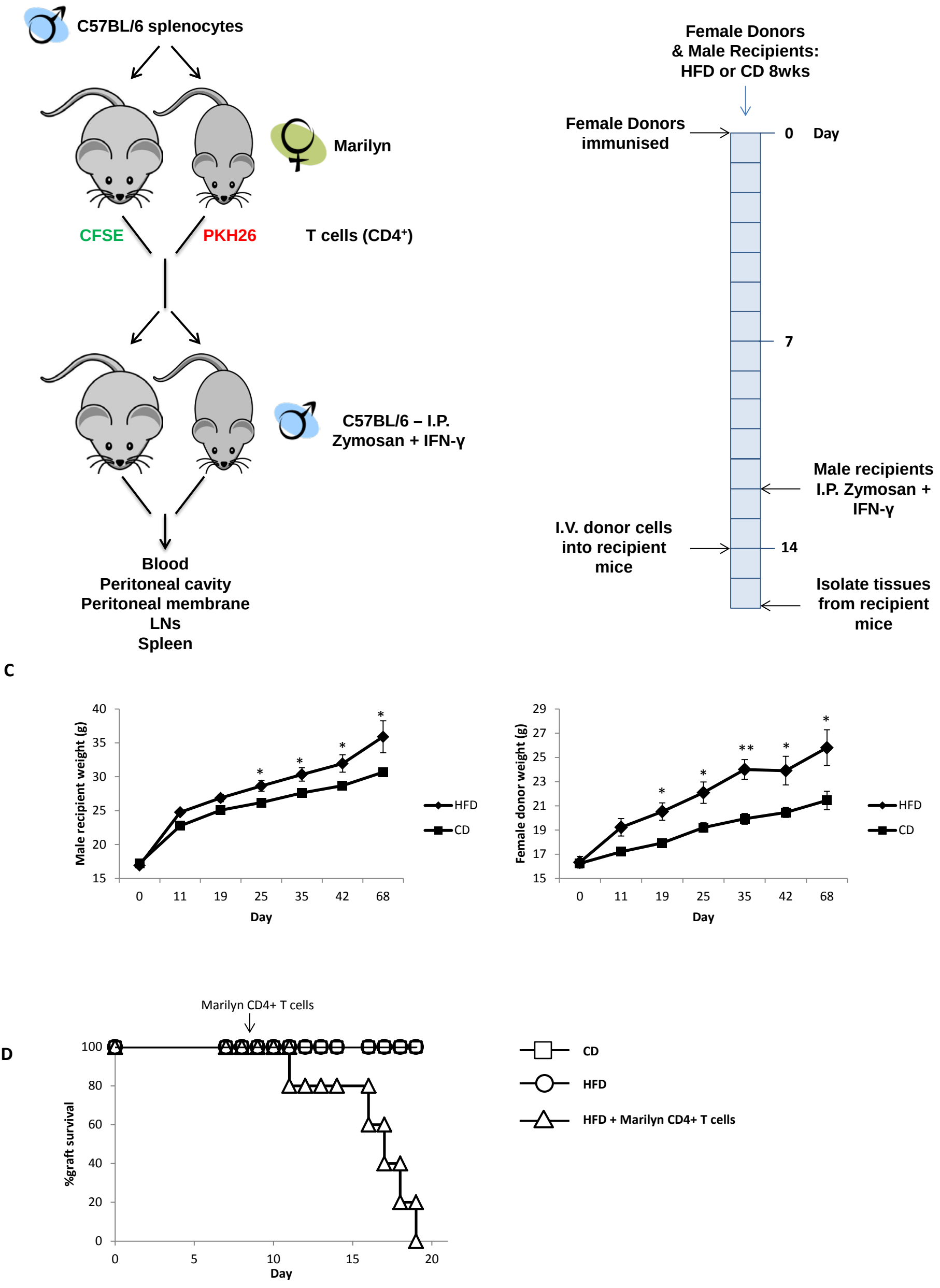
A
C57BL/6 splenocytes
Marilyn
CFSE
PKH26
T cells (CD4+)
C57BL/6 – I.P.
Zymosan + IFN-γ
Blood
Peritoneal cavity
Peritoneal membrane
LNs
Spleen
B
Female Donors
& Male Recipients:
HFD or CD 8wks
Female Donors
immunised
0
Day
7
Male recipients
I.P. Zymosan +
IFN-γ
I.V. donor cells
into recipient
mice
14
Isolate tissues
from recipient
mice
C
Male recipient weight (g)
Day
HFD
CD
Female donor weight (g)
Day
HFD
CD
D
Marilyn CD4+ T cells
%graft survival
Day
CD
HFD
HFD + Marilyn CD4+ T cells

Figure S2

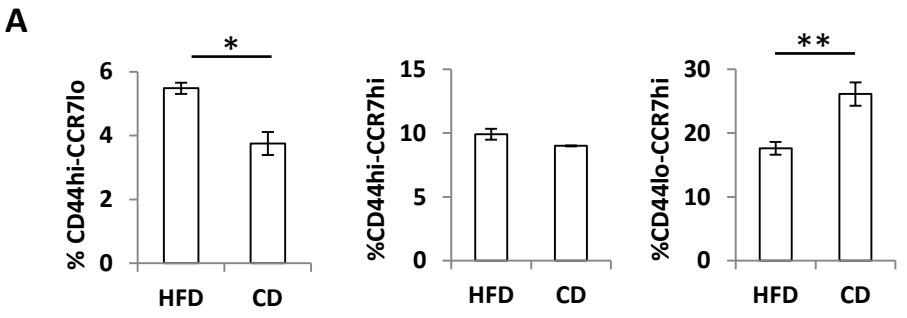
A
% CD44hi-CCR7lo
%CD44hi-CCR7hi
%CD44lo-CCR7hi
HFD
CD
*
**

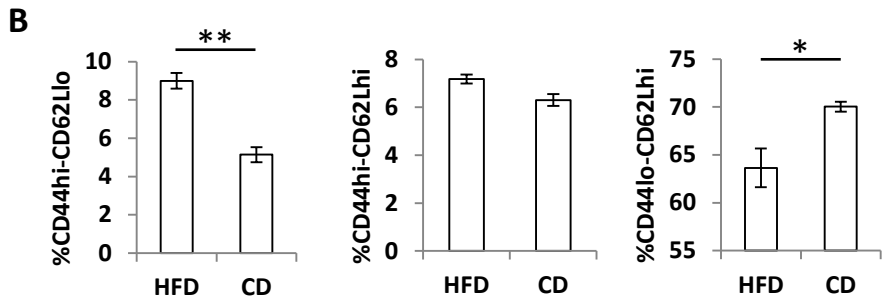
B
%CD44hi-CD62Llo
%CD44hi-CD62Lhi
%CD44lo-CD62Lhi
HFD
CD
**
*

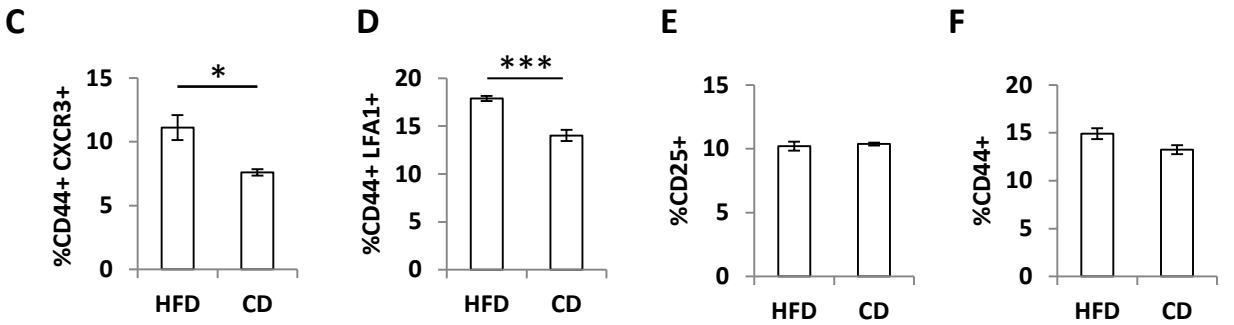
C
%CD44+ CXCR3+
D
%CD44+ LFA1+
E
%CD25+
F
%CD44+
HFD
CD
*
***

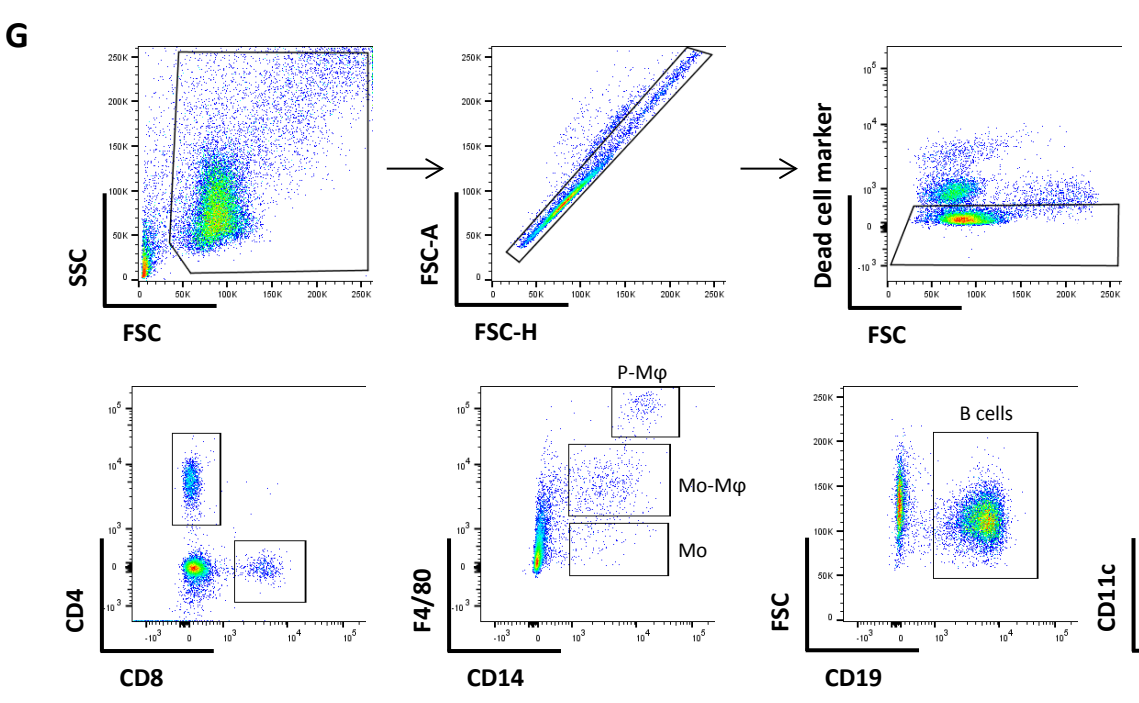
G
SSC
FSC
FSC-A
FSC-H
Dead cell marker
FSC
CD4
CD8
P-Mφ
Mo-Mφ
Mo
F4/80
CD14
FSC
CD19
B cells
CD11c
MHC II
DC

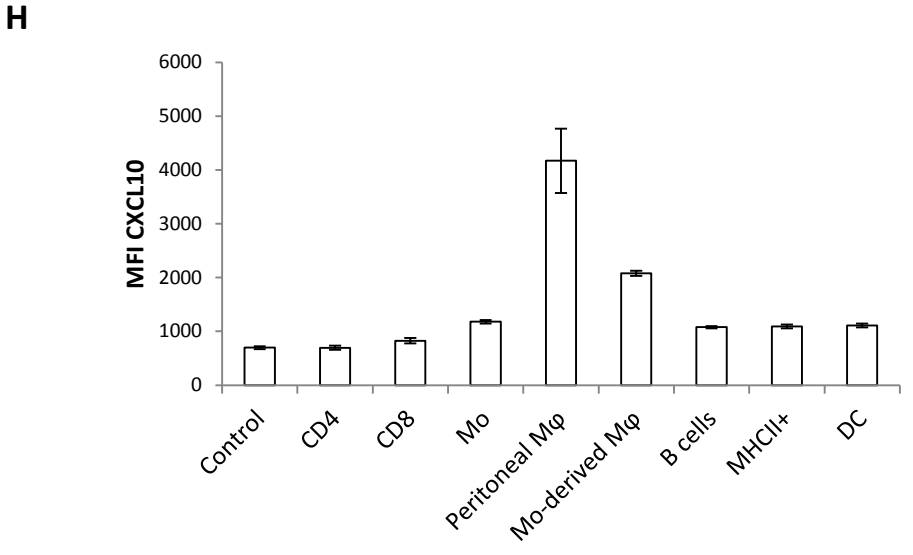
H
MFI CXCL10
Control
CD4
CD8
Mo
Peritoneal Mφ
Mo-derived Mφ
B cells
MHCII+
DC

Figure S3

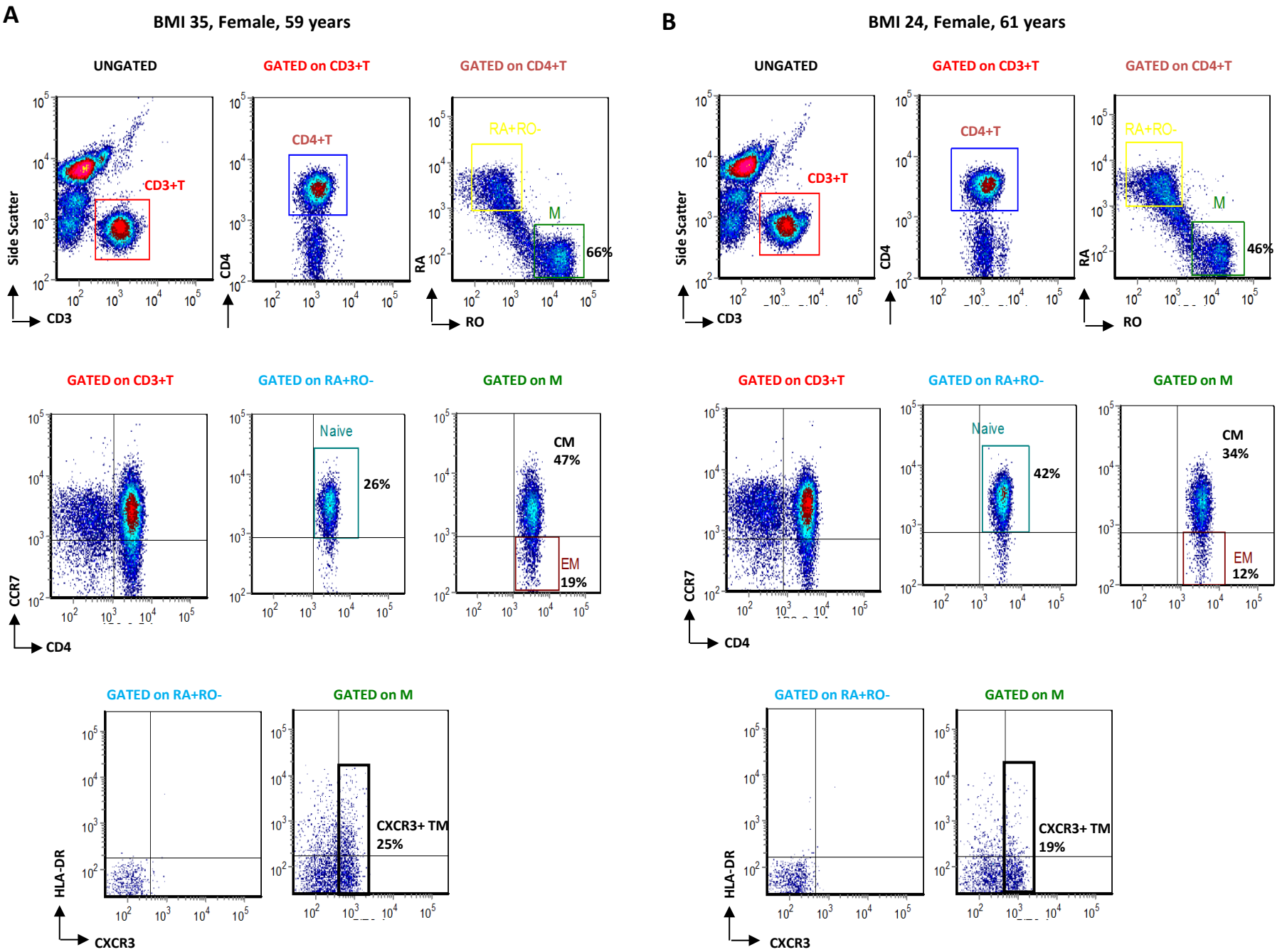
A
BMI 35, Female, 59 years
UNGATED
GATED on CD3+T
GATED on CD4+T
Side Scatter
CD3
CD3+T
CD4
CD4+T
RA
RO
RA+RO-
M
66%
GATED on CD3+T
GATED on RA+RO-
GATED on M
CCR7
CD4
Naive
26%
CM
47%
EM
19%
GATED on RA+RO-
GATED on M
HLA-DR
CXCR3
CXCR3+ TM
25%
B
BMI 24, Female, 61 years
UNGATED
GATED on CD3+T
GATED on CD4+T
Side Scatter
CD3
CD3+T
CD4
CD4+T
RA
RO
RA+RO-
M
46%
GATED on CD3+T
GATED on RA+RO-
GATED on M
CCR7
CD4
Naive
42%
CM
34%
EM
12%
GATED on RA+RO-
GATED on M
HLA-DR
CXCR3
CXCR3+ TM
19%

Figure S4

A

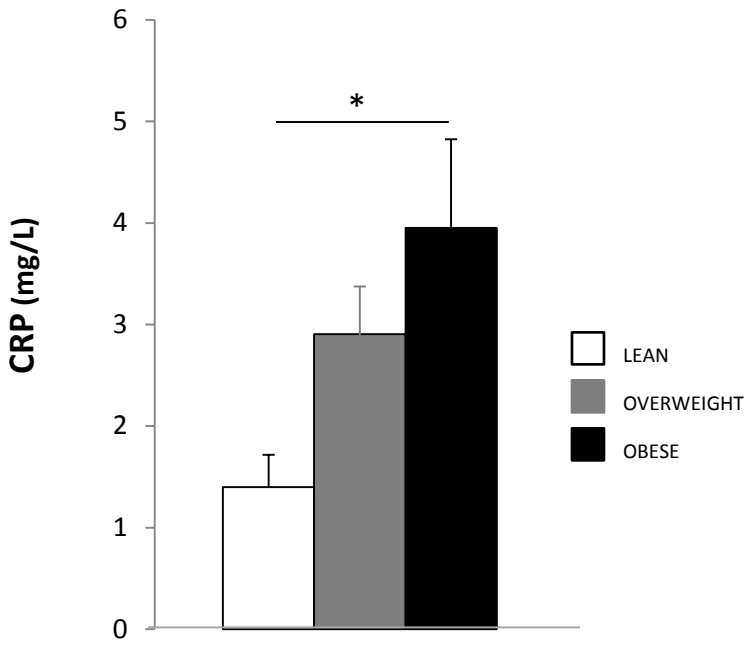

B

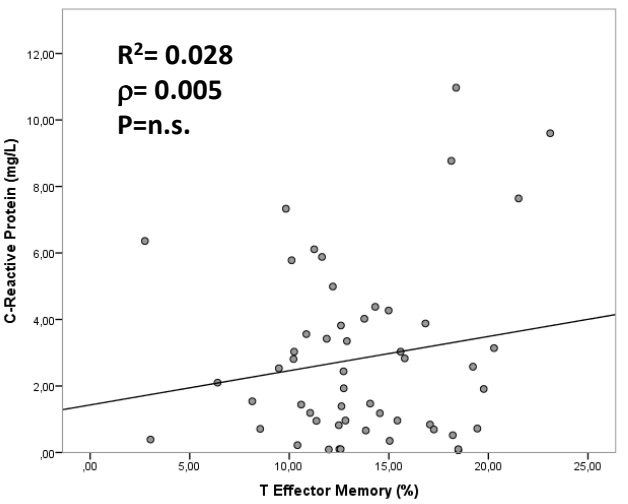

C

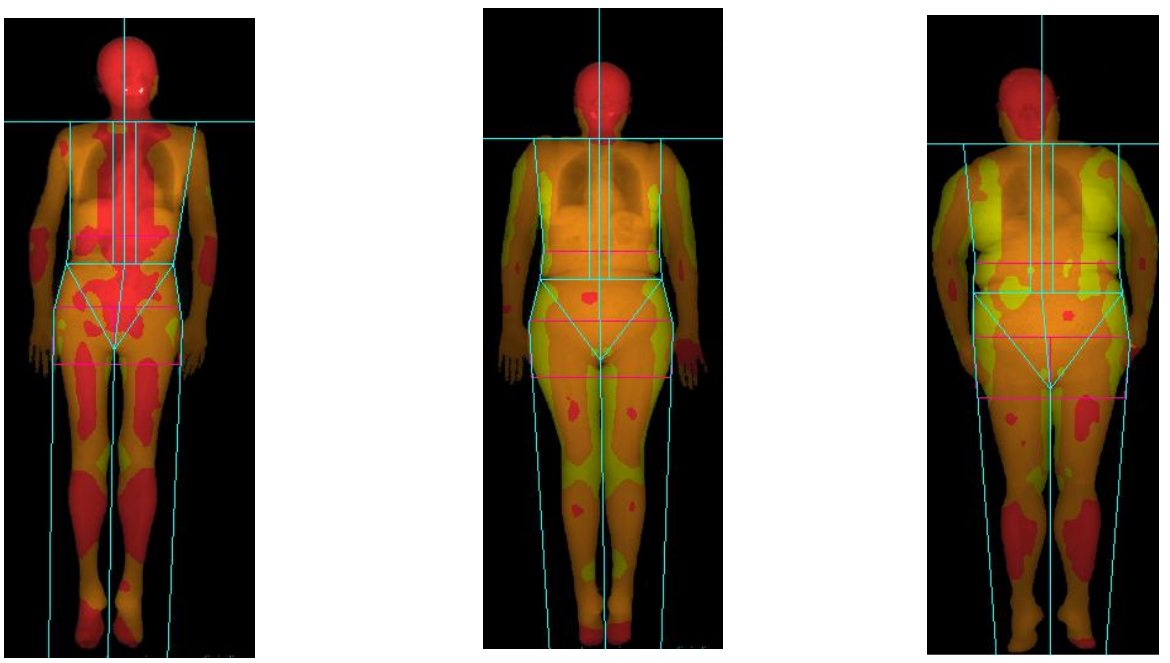

LEAN

Female 66 years
BMI: 19.2 Kg/m²
Android fat: 25.2%
Gynoid fat: 36.4 %
A/G_r : 0.69

OVERWEIGHT

Female 66 years
BMI: 26.2 Kg/m²
Android fat: 51.2%
Gynoid fat: 54.3 %
A/G_r : 0.94

OBESE

Female 66 years
BMI: 37.8 Kg/m²
Android fat: 63.4%
Gynoid fat: 52.4 %
A/G_r : 1.21

D

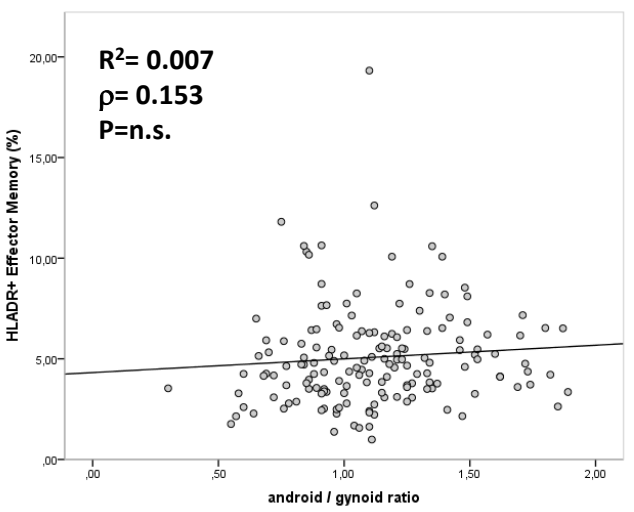

E

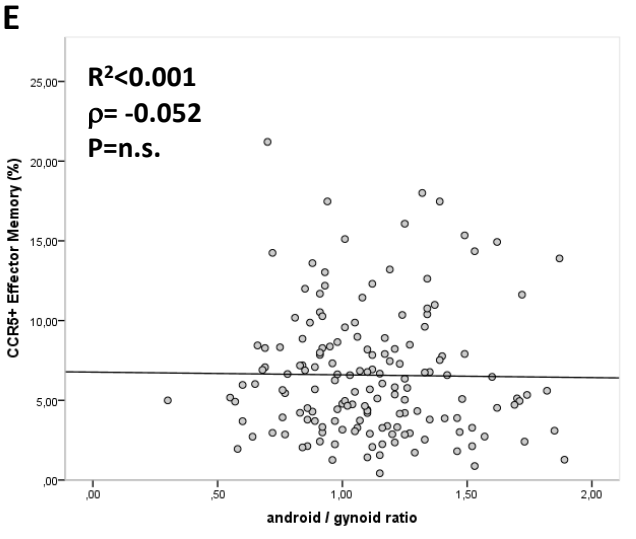

Figure S5

A

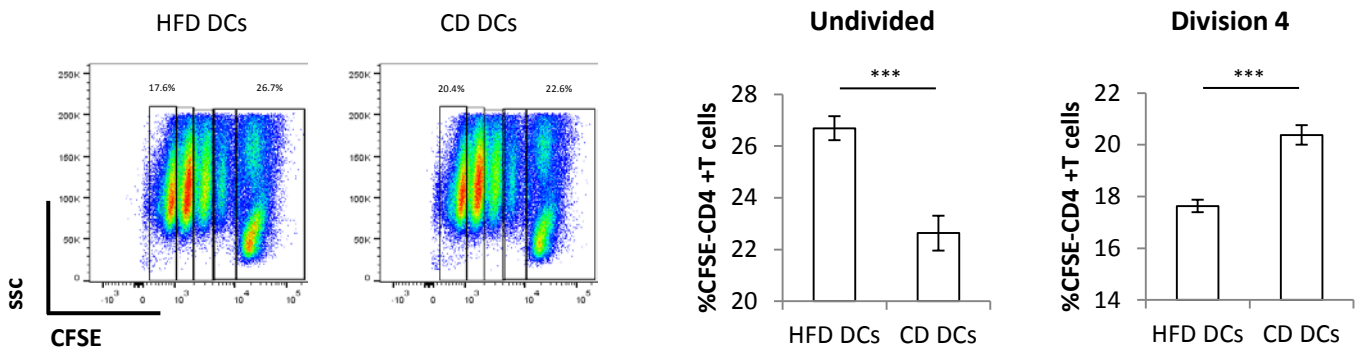

B

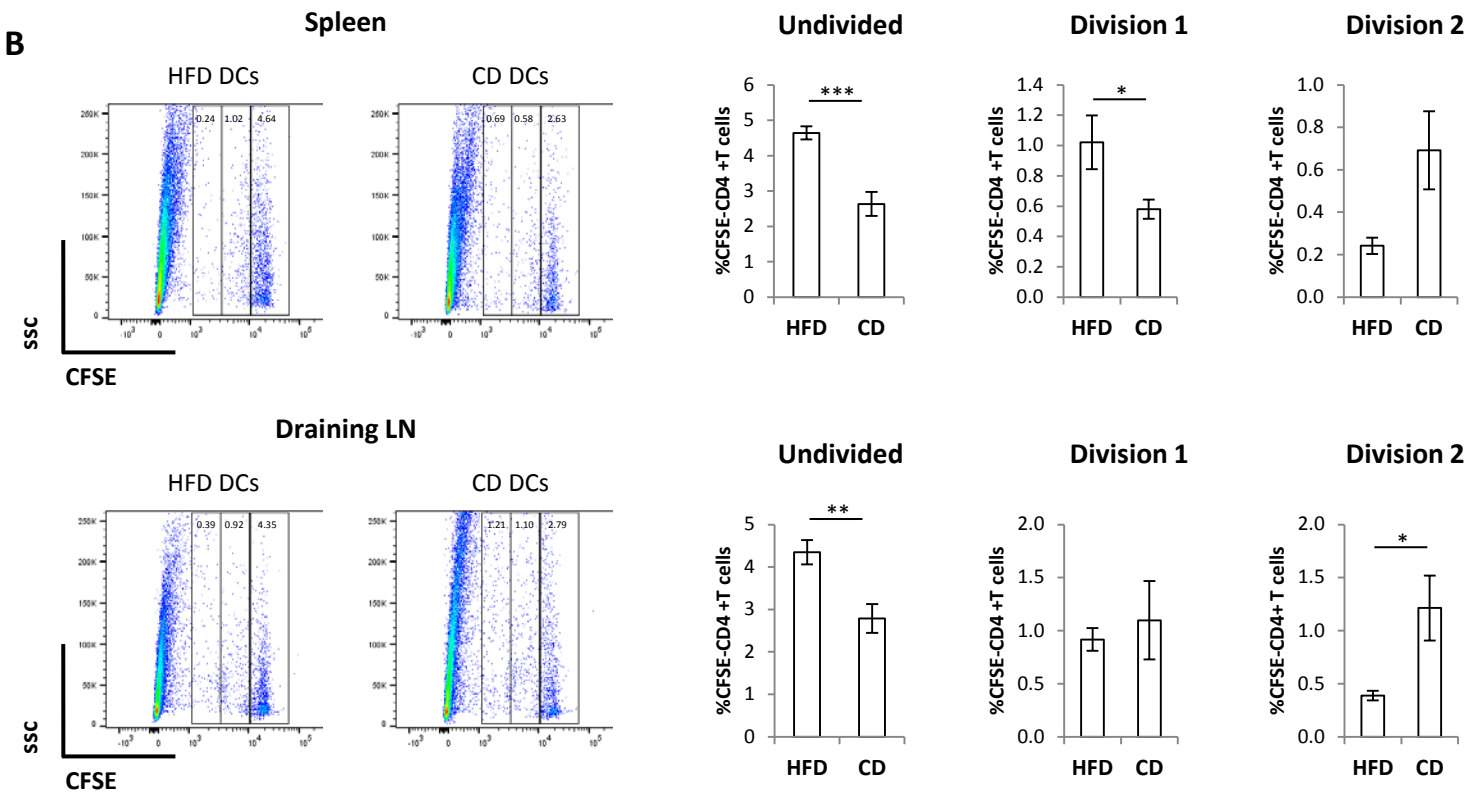

C

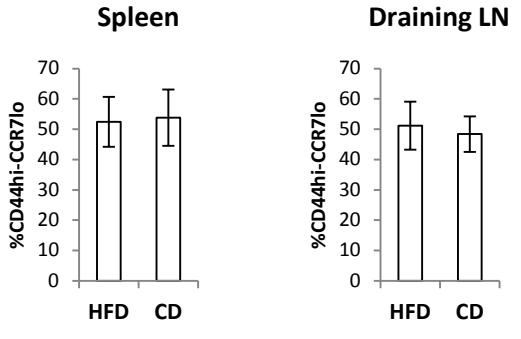

Figure S6

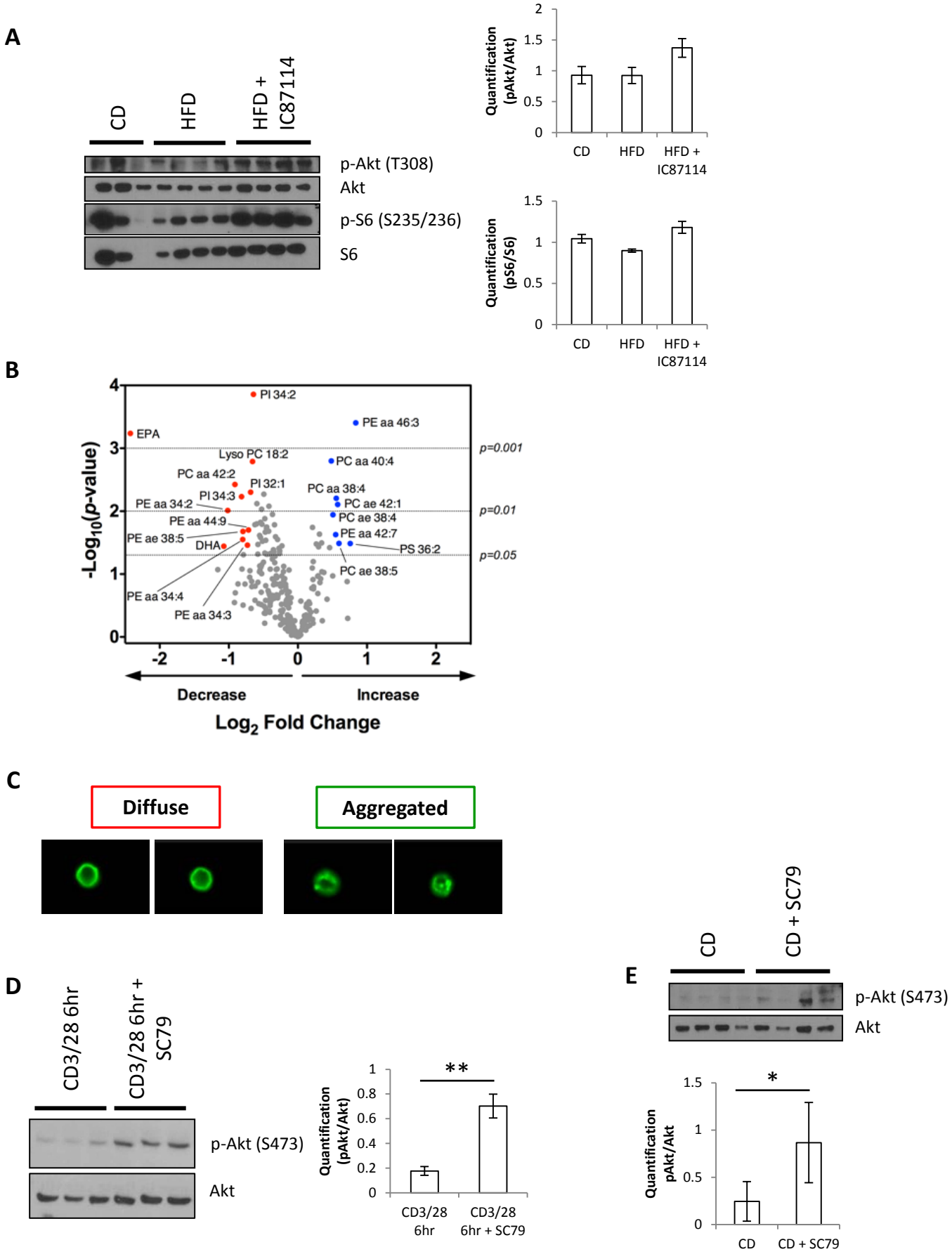
A
CD
HFD
HFD + IC87114
p-Akt (T308)
Akt
p-S6 (S235/236)
S6
Quantification (pAkt/Akt)
Quantification (pS6/S6)
B
-Log10(p-value)
Log2 Fold Change
Decrease
Increase
p=0.001
p=0.01
p=0.05
PI 34:2
PE aa 46:3
EPA
Lyso PC 18:2
PC aa 40:4
PC aa 42:2
PI 32:1
PC aa 38:4
PI 34:3
PC ae 42:1
PE aa 34:2
PC ae 38:4
PE aa 44:9
PE aa 42:7
PE ae 38:5
DHA
PS 36:2
PC ae 38:5
PE aa 34:4
PE aa 34:3
C
Diffuse
Aggregated
D
CD3/28 6hr
CD3/28 6hr + SC79
p-Akt (S473)
Akt
Quantification (pAkt/Akt)
**
CD3/28 6hr
CD3/28 6hr + SC79
E
CD
CD + SC79
p-Akt (S473)
Akt
Quantification pAkt/Akt
*

Table S1

	LEAN (N= 370)	OVERWEIGHT (N= 552)	OBESE (N= 250)	P
Age (yrs)	*67 (46-78)*	*68 (52-78)*	*70 (56-78)*	**< 0.001**
Gender (men/women)	*111/259*	*281/271*	*90/160*	
BMI (Kg/m²)	*22.90 (20.20-24.60)*	*27.10 (25.30-29.10)*	*32.10 (30.40-37.43)*	**< 0.001**
Total cholesterol (mg/dL)	*207.00 (162.00-250.00)*	*201.00 (155.00-250.00)*	*198.00 (151.00-243.00)*	0.279
HDL-C (mg/dL)	*67.00 (48.80-90.00)*	*57 (42-81)*	*57 (40-73)*	**< 0.001**
Triglycerides (mg/dL)	*77 (50-139.4)*	*96 (56-163)*	*99 (64-182)*	**< 0.001**
LDL-C (Friedewald Formula)	*119.2 (81.56-158.8)*	*118.20 (80.92-167.48)*	*118.80 (77.26-158.72)*	0.714
ApoA-I (mg/dL)	*165 (125.8-179)*	*154 (115.7-175)*	*151 (115-174)*	**< 0.001**
Apo-B (mg/dL)	*99 (83-131)*	*101 (79.6-134)*	*99 (81-128)*	0.712
Fasting glucose levels (mg/dL)	*88 (75-104)*	*93 (80-114)*	*100 (84-133)*	**< 0.001**
Total leukocytes (x10³ U/L)	*5.71 (4.33-8.20)*	*6.36 (4.74-8.80)*	*6.39 (4.71-8.82)*	**< 0.001**
Neutrophils (x10³ U/L)	*3.31 (2.12-5.12)*	*3.56 (2.43-5.39)*	*3.59 (2.38-5.33)*	**0.010**
Lymphocytes (x10³ U/L)	*1.78 (1.13-2.55)*	*1.92 (1.36-2.73)*	*1.95 (1.32-2.77)*	**< 0.001**
Monocytes (x10³ U/L)	*0.49 (0.34-0.75)*	*0.56 (0.39-0.80)*	*0.55 (0.38-0.81)*	**0.002**
Eosinophils (x10³ U/L)	*0.12 (0.05-0.27)*	*0.15 (0.07-0.33)*	*0.16 (0.07-0.33)*	0.062
Basophils (x10³ U/L)	*0.03 (0.01-0.05)*	*0.03 (0.01-0.05)*	*0.03 (0.05)*	0.668

Table S2

	High Fat diet (HFD)	**Chow diet (CD)**	**Palmitate-enriched diet (PED)**	**Palmitate-control diet (PCD)**
Fat (%)	***34.9***	***9.1***	***25.2***	***4.2***
Cholesterol, ppm	*301*	*200*	*0*	*0*
Linoleic Acid (%)	*4.7*	*2.32*	*3.86*	*1.89*
Linolenic Acid (%)	*0.39*	*0.21*	*0.29*	*0.29*
Arachidonic Acid (%)	*0.06*	*0.02*	*0*	*0*
Omega-3 Fatty Acids (%)	*0.39*	*0.32*	*0.29*	*0.21*
Total Saturated (%)	*13.68*	*2.72*	*10.05*	*0.39*
Total Mono-saturated (%)	*14*	*2.88*	*10.38*	*1.56*
Polyunsaturated (%)	-	-	*4.38*	*2.07*
Energy (kcal/g)[2]	***5.1***	***3.56***	***4.83***	***3.78***
Protein (%)	*18.1*	*23*	*13*	*16.7*
Fat (%)	*61.6*	*22*	*47*	*10*
Carbohydrate (%)	*20.3*	*55*	*40*	*73.3*

Supplemental Figures and Tables Legends

Supplemental Figure 1 (related to Fig 1). *In vivo* peritoneal recruitment and Rag2KO skin grafts. (A-B) Schematic of the design **(A)** and timeline **(B)** of the *in vivo* peritoneal recruitment model used in Fig 1A-D. **(C)** Weight gain curves of mice over the 8 weeks HFD or CD in C57Bl/6 male recipients and Marilyn female donors. **(D)** Survival curve of C57Bl/6 male skin grafts on HFD or CD Rag2KO female recipients up to 21 days post-transplantation. Also shown is the survival curve following reconstitution of HFD Rag2KO mice with $CD4^+$ T cells isolated from Marilyn female mice**. (C-D)** n=3-6 independent mice. **(C)** Values denote mean ± s.e.m. *P<0.05; **P<0.01.

Supplemental Figure 2 (related to Fig 2). HFD-induced differentiation of $CXCR3^+$-$LFA1^+$ effector memory-like phenotype in mice and *in vivo* sources of CXCL10. (A-F) Cell surface staining of CD25, CD44, CCR7, CD62L, CXCR3 and LFA1 in *in vivo*-primed $CD4^+$ T cells isolated from pooled lymph nodes of the HFD or CD Marilyn female donor mice used in Fig 1A-D (%). **(G)** Gating strategy defining immune cells tested for expression of CXCL10 in the peritoneal cavity 48 hours after *i.p.* injection of IFNγ (600U/mouse). **(H)** MFI of CXCL10 in the immune cell types defined in G. **(A-F)** n=4-6 independent donors. **(H)** n=2 independent mice. **(A-F)** Values denote mean ± s.e.m. *P<0.05; **P<0.01; *** P<0.001.

Supplemental Figure 3 (related to Fig 3). Flow cytometry gating strategy to identify $CD4^+$ T cell subsets in humans. Examples of the gating strategy used in an obese **(A)** and a lean **(B)** individual to identify the principal $CD4^+$ T cell subsets and some of the T cell subpopulations in the peripheral blood samples of lean, over-weight and obese subjects.

Supplemental Figure 4 (related to Fig 3). Body fat distribution association with inflammatory T cell subsets and inflammatory mediators. (A-B) Levels of CRP in the

blood of lean, over-weight and obese subjects stratified according to BMI **(A)** and correlation of CRP with effector memory T cells **(B)**. **(C)** Body mass fat distribution of android and gynoid fat within a lean, overweight and obese individual (analysed with body composition by dual-energy X-ray absorptiometry, DEXA). **(D-E)** Correlation of $HLADR^+$ **(D)** and $CCR5^+$ effector memory T cells **(E)** with android/gynoid ratio. **(A-B, D-E)** n=187. ANCOVA, *P<0.05.

Supplemental Figure 5 (related to Fig 4). Dendritic cells from HFD-fed mice do not affect T cell differentiation. (A) Dot plots and quantification of *in vitro* proliferation of CFSE-labelled $CD4^+$ T cells isolated from pooled lymph nodes of CD Marilyn female mice incubated with $CD11c^+$ DC isolated from the spleen of HFD or CD C57Bl/6 male mice for 3 days. Undivided and 4^{th} division populations are quantified by dilution of the CFSE-label. **(B)** Dot plots and quantification of *in vivo* proliferation of CFSE-labelled $CD4^+$ T cells isolated from pooled lymph nodes of CD Marilyn female *i.v.* injected into C57Bl/6 female recipient mice in combination with $CD11c^+$ dendritic cells isolated from the spleen of HFD or CD C57Bl/6 male mice *i.p.* injected for 5 days. Undivided, 1^{st} and 2^{nd} division populations are quantified from the spleen and mesenteric lymph nodes of recipient females by dilution of the CFSE-label. **(C)** Cell surface staining of CD44 and CCR7 in the population of CFSE-labelled $CD4^+$ T cells isolated *in vivo* from the spleen and mesenteric lymph nodes of the C57Bl/6 recipient female mice. **(A)** n=3 independent mice (each mouse was tested in triplicate). **(B-C)** n=4 independent mice. Values denote mean ± s.e.m. *P<0.05; ** P<0.01; ***P<0.001.

Supplemental Figure 6 (related to Fig 5 and 6). Mechanistic insights in to saturated FA-induced effector memory differentiation of $CD4^+$ T cells. (A) Levels and densitometric quantification of p-Akt (T308), Akt, p-S6 (S235/236) and S6 protein expression in *in vivo*-primed $CD4^+$ T cells isolated from mesenteric lymph nodes of CD and HFD mice *i.p.* injected with the PI3K inhibitor IC87114 or left untreated. **(B)** Volcano plot of fatty acids and phospholipids detected in in *in vivo*-primed $CD4^+$ T cells isolated from mesenteric lymph

nodes of CD and HFD mice. Fifteen fatty acids were detected including palmitic acid C16:0; palmitoleic acid C16:1; margaric acid C17:0; stearic acid C18:0; oleic acid C18:1; linoleic acid C18:2; γ-linolenic acid C18:3; arachic acid C20:0; arachidonic acid C20:4; eicosapentaenoic acid C20:5 (EPA); behenic acid C22:0; erucic acid C22:1; docosahexaenoic acid C22:6 (DHA); lignoceric acid C24:0; nervonic acid C24:1. Out of 356 phospholipids analyzed (including LysoPC: lysophosphatidylcholine; PC: phosphatidylcholine; PC aa: phosphatidylcholine acyl-acyl; PC ae: phosphatidylcholine acyl-alkyl also known as plasmalogens; PE: phosphatidylethanolamine; PE aa: phosphatidylethanolamine acyl-acyl; PE ae: phosphatidylethanolamine acyl-alkyl also known as plasmalogens; PS: phosphatidylserines; LysoPI: lysophosphatidylinositol; PI: phosphatidylinositol; PG: phosphatidylglycerol; LysoPA: lysophosphatidic acid; PA: phosphatidic acid; SM: sphingomyelin; Cer: ceramide; GCer: glucosyl/galactosyl-ceramide; LacCer: lactosyl-ceramide and gangliosides GM1, GM2 and GM3) 229 different species belonging to different families were detected. The volcano plot displays the relationship between fold-change (expressed as log2) and significance between the two groups (CD vs. HFD), using a scatter plot view. The y-axis is the negative log10 of p values (a higher value indicates greater significance as indicated by dashed lines) and the x-axis is the difference in levels of metabolites between two experimental groups. Significantly increased metabolites are shown by blue dots while red dots represented those decreased. **(C)** Representative fluorescence images of the aggregation of CTxB signal. **(D)** Levels and densitometric quantification of p-Akt (S473) and Akt protein expression in $CD4^+$ T cells isolated from pooled lymph nodes of mice, then activated with plate bound anti-CD3 (0.5µg/ml, ebioscience) and anti-CD28 (2.5µg/ml, ebioscience) for 6hrs in the presence or absence of the Akt activator SC79 (500 nM). **(E)** Levels and densitometric quantification of p-Akt (T308) and Akt protein expression in *in vivo*-primed $CD4^+$ T cells isolated from mesenteric lymph nodes of CD mice *i.p.* injected with the Akt activator SC79 or left untreated. **(A, D-E)** Each lane shows data from independent mouse samples. **(B)** n=3 independent mice. Values denote mean ± s.e.m. *P<0.05; **P<0.01.

Supplemental Table 1 (related to Fig 3). Parameters analysed in the n=1,172 subjects selected. All the variables were non-normally distributed (Kolmogorov-Smirnov test). Median (Interquartile-Range, IQR) are presented for each variable across subjects divided into lean (BMI< 25 Kg/m^2), overweight (BMI≥ 25 Kg/m^2) and obese (BMI < 30 Kg/m^2). Grubb's test was performed for detection of outliers (below and above 1.5∗IQR) for each distribution. P is derived from Analysis of covariance (ANCOVA) adjusting for age, gender and therapies.

Supplemental Table 2 (related to Fig 1, 2 and 4-7). Nutrients and caloric composition of diets: HFD, CD, PED and PCD.

Supplemental Experimental Procedures

Determination of abdominal adiposity (android/gynoid ratio)

Total body DXA scans were acquired using Lunar iDXA (GE Healthcare, Madison, WI). Daily quality control scans were acquired during the study period. All subjects were scanned while wearing a hospital gown with all metal artifacts removed from their body. Trained operators, blinded on patient's identity and clinical history, performed all scans. Patient positioning and data acquisition was conducted in accordance to the operator's manual. Lunar iDXA scans were analyzed with the enCORE software (version 14.0), (GE Healthcare, Madison, WI), (Rothney et al., 2013). Out of total weight, the software allows to discriminate the bone mass, the fat mass and the lean mass. DXA android fat was computed automatically over the DXA android region, a region-of-interest automatically defined by the enCORE software, whose caudal limit is automatically placed at the top of the iliac crest and whose height is set to 20% of the distance from the top of the iliac crest to the base of the

skull to define its cephalad limit. DEXA gynoid fat was computed automatically as well, over the DXA gynoid region (percent of fat tissue in inferior half abdominal, glutei and femoral regions); their ratio is automatically determined by the software to give the gender-adjusted measure of abdominal obesity (Rothney et al., 2013).

Lipidomic profile by liquid chromatography-tandem mass spectrometry (LC-MS/MS)

All HPLC solvents were MS grade (Carlo Erba); fatty acid internal standards ^{13}C-labelled palmitic acid (C16:0) and ^{13}C-labelled linoleic acid (C18:2) were purchased from Sigma. Phospholipid standards: C13:0 lysophosphatidylcholines (LPC); C:25:0 phosphatidylcholines (PC); C12:0 sphingomyelin (SM); 12:0-13:0 phosphatidylserine (PS); 12:0-13:0 phosphatidylinositol (PI); 12:0-13:0 phosphatidylglycerol (PG); 12:0-13:0 phosphatidic acid (PA); 12:0-13:0 phosphatidylethanolamine (PE); C12 ceramide (Cer); glucosyl (β) C12 ceramide (GC); lactosyl (β) C12 ceramide (LacCer); C17 mono-sulfo galactosyl-(β)-ceramide (D18:1/17:0; GalCer); were purchased from Avanti Polar Lipids. Quantification of fifteen different fatty acids was performed as previously described (Cermenati et al., 2015). Briefly, samples were homogenized in methanol:acetonitrile (1:1). Aliquots of extracts, after addition of internal standards (^{13}C-labelled palmitic and linoleic acids), were subjected to acid hydrolysis and processed as previously described (Cermenati et al., 2015). Fatty acid quantification was performed on a API-4000 triple quadrupole mass spectrometer (AB Sciex) coupled with a HPLC system (Agilent) and CTC PAL HTS auto-sampler (PAL System) using standard curves for each fatty acid analyzed. For the quantification of the different phospholipids, the MS analysis was performed with a flow injection analysis-tandem mass spectrometry (FIA-MS/MS) method. The identity and quantification of the different phospholipids were confirmed using pure standards. Methanolic:acetonitrile extracts were analyzed by a 5 min run in both positive and negative ion mode with a 268 multiple reaction monitoring (MRM) transition in positive mode and 88

MRM transition in negative mode. An ESI source connected with an API 4000 triple quadrupole instrument (AB Sciex) was used. The mobile phase was 0.1 % formic acid in MeOH for FIA positive analysis and 5 mM ammonium acetate pH 7 in MeOH for FIA negative. MultiQuant™ software version 3.0.2 was used for data analysis and peak review of chromatograms. Each metabolite level detected was normalized on protein content.